Evaluation of ferrocenyl-containing γ-hydroxy-γ-lactam-derived tetramates as potential antiplasmodials

Nicolas Chopin, Julien Bosson, Shinya Iikawa, Stéphane Picot, Anne-Lise Bienvenu, Adeline Lavoignat, Guillaume Bonnot, Mickaël Riou, Corinne Beaugé, Vanaïque Guillory, et al.

Evaluation of ferrocenyl-containing γ-hydroxy-γ-lactam-derived tetramates as potential antiplasmodials [≠]

Nicolas Chopin,[a] Julien Bosson,[a] Shinya Iikawa,[a] Stéphane Picot,[a,b] Anne-Lise Bienvenu,[a,c] Adeline Lavoignat,[a] Guillaume Bonnot,[a] Mickael Riou,[d] Corinne Beaugé,[d] Vanaïque Guillory,[d,e] Christophe Biot,[f] Guillaume Pilet,[g] Matthieu Chessé,[h] Elisabeth Davioud-Charvet,[h,*] Mourad Elhabiri,[h,*] Jean-Philippe Bouillon,[i,*] and Maurice Médebielle[a,*]

[a] *Univ. Lyon, Université Lyon 1, CNRS, INSA, CPE-Lyon, ICBMS, UMR 5246, Villeurbanne, France*

[b] *Institut de Parasitologie et Mycologie Médicale, Groupement Hospitalier Nord, Hospices Civils de Lyon, Lyon, France*

[c] *Service Pharmacie, Groupement Hospitalier Nord, Hospices Civils de Lyon, Lyon, France*

[d] *INRAE, UE-1277 Plateforme d'Infectiologie Expérimentale (PFIE), Centre Val de Loire, Nouzilly, France*

[e] *INRAE, UMR-1282 Infectiologie et Santé Publique (ISP) , Centre Val de Loire – Université de Tours, Nouzilly, France*

[f] *Université de Lille, CNRS, UMR 8576, UGSF, Unité de Glycobiologie Structurale et Fonctionnelle, Lille, France*

[g] *Univ. Lyon, Université Lyon 1, CNRS, LMI, UMR 5615, Villeurbanne, France*

[h] *UMR 7042 Université de Strasbourg–CNRS–UHA, Laboratoire d'Innovation Moléculaire et Applications (LIMA), Team Bio(IN)organic and Medicinal Chemistry, European School of Chemistry, Polymers and Materials (ECPM), 25 Rue Becquerel, F-67087 Strasbourg, France*

[i] *Normandie Université, COBRA, UMR 6014 et FR 3038, Université de Rouen, INSA Rouen, CNRS, Mont Saint-Aignan, France*

*Corresponding author. E-mail: maurice.medebielle@univ-lyon1.fr

*Co-corresponding author. E-mail: jean-philippe.bouillon@univ-rouen.fr

*Co-corresponding author. E-mail: elhabiri@unistra.fr

[≠] Dedicated to the memory of Professor Maurizio Botta

A series of ferrocenyl-containing γ-hydroxy-γ-lactam tetramates were prepared in 2-3 steps through ring opening-ring closure (RORC) process of γ-ylidene-tetronate derivatives in the presence of ferrocenyl alkylamines. The compounds were screened *in vitro* for their antiplasmodial activity against chloroquine-sensitive (3D7) and chloroquine-resistant (W2) clones of *P. falciparum*, displaying activity in the range of 0.12-100 µM, with generally good resistance index. The most active ferrocene in these series exhibited IC_{50} equal to 0.09 µM (3D7) and 0.12 µM (W2). The low cytotoxicity of the ferrocenyl-containing γ-hydroxy-γ-lactam tetramates against Human Umbilical Vein Endothelial (HUVEC) cell line demonstrated selective antiparasitic activity. The redox properties of these ferrocene-derived tetramates were studied and physico-biochemical studies evidenced that these derivatives can exert potent antimalarial activities *via* a mechanism distinct from ferroquine.

Key words: antimalarial, tetramate, ferrocene, lactam, Fenton, ROS

1. Introduction

Malaria is a disease endemic in tropical and subtropical parts of the world. Despite recent progress toward malaria elimination in few endemic areas, it is estimated that half of the world population is currently at risk of malaria disease, and *P. falciparum* parasite is responsible for a significant child death toll [1]. The widespread resistance of *P. falciparum* parasites to current drugs, causes an urgent need for new classes of antimalarial drugs that are either derived from known drugs [2-5] or that operate by novel mechanism of actions [6]. The current recommended first-line malaria treatment in most endemic areas are artemisinin-based combined therapies (ACTs) [7]. In our current research program directed towards the synthesis and biological evaluation of new antimalarials, we have previously reported on the synthesis of a set of γ-hydroxy-γ-lactam derived-tetramates bearing a 7-chloro-4-aminoquinoline skeleton of general structure **1** [8]. *In vitro* antimalarial activity of these new γ-lactams was measured using *P. falciparum* clones [9] of different sensitivities (3D7 and W2) and they were found to be active in the range of 14-827 nM with generally good resistance index. Tetramate derivatives **2** and **3** were the most promising compounds with **2** being more active than reference chloroquine (**CQ**) (Figure 1). While synthetic antimalarials having a γ-lactam or pyrrolone skeleton have been scarcely explored [10], one can argue that molecules of general structure **1** are chloroquine-like structures and they may in part act through inhibition of hemozoin formation [11] as **CQ**. Since these tetramates are obtained easily through ring opening-ring closure (RORC) process of

readily available γ-ylidene-tetronates [12] in the presence of amines [8], our next goal was to screen synthetic or commercially available amines in an effort to identify new potent tetramates not bearing a 4-aminoquinoline skeleton. From these screening experiments, ferrocenyl-containing γ-hydroxy-γ-lactam tetramates were discovered as the most potent molecules. Ferroquine (**FQ**, Figure 2) [13], a ferrocene-quinoline hybrid is a very potent antimalarial currently in phase IIb clinical trials in combination with Artefenomel (a synthetic trioxolane) [14]. Ferroquine is believed to exert its antiplasmodial activity via oxidative stress generated from the redox activity of the ferrocenyl moiety and through inhibition of hemozoin formation. Analogues of Ferroquine and ferrocene-containing hybrids have been synthesized for years and evaluated as antiplasmodials [15] and ferrocene is a valuable motif recurring in diverse chemical classes of antiparasitic compounds [16-18]. However, to the best of our knowledge, there has been no report on the synthesis and evaluation as potent antimalarials of ferrocenyl-containing γ-lactams.

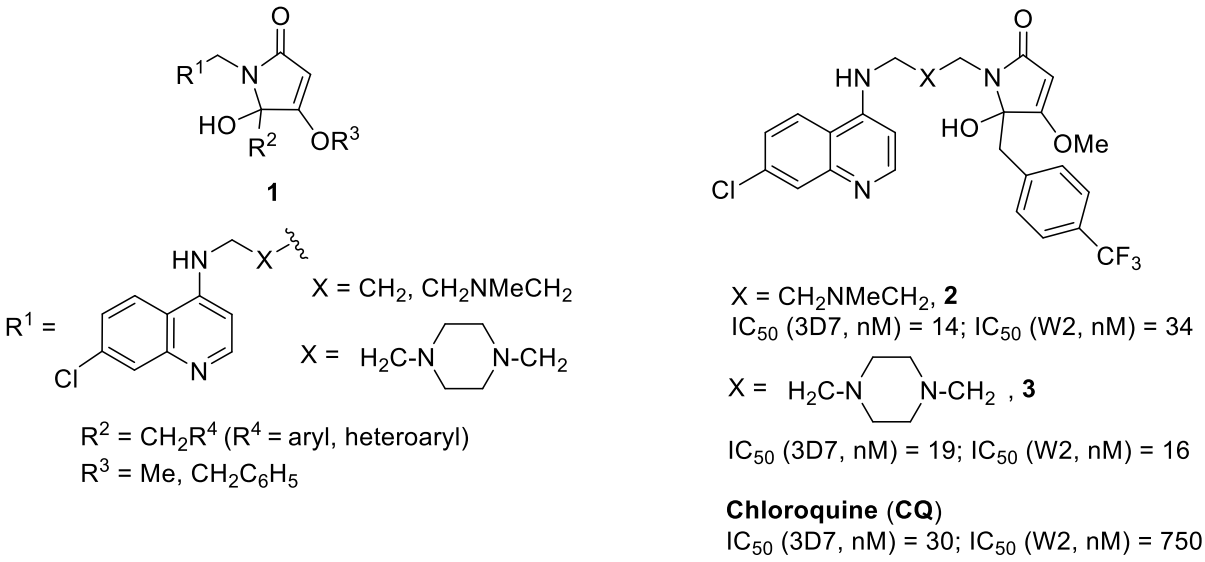

Figure 1. Chemical structures of our previous 7-chloro-4-aminoquinoline-γ-hydroxy-γ-lactam derived-tetramates [8].

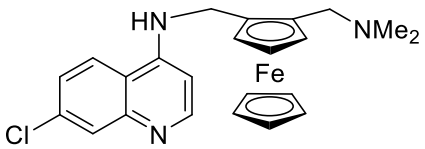

Figure 2. Chemical structure of **Ferroquine** (**FQ**)

2. Results and discussion

*2.1. Synthesis of γ-ylidene-tetronate derivatives **12-19** and ferrocenyl-containing γ-hydroxy-γ-lactam tetramates **20-37***

γ-Ylidene-tetronates **12-19** were obtained through the condensation of methyl and benzyl tetronates **4a-b** (methyl tetronate **4a** being commercially available) with heteroaryl aldehydes **5-11**, in a 2-steps aldolisation/dehydration sequence recently disclosed in our laboratory (Scheme 1) [12].

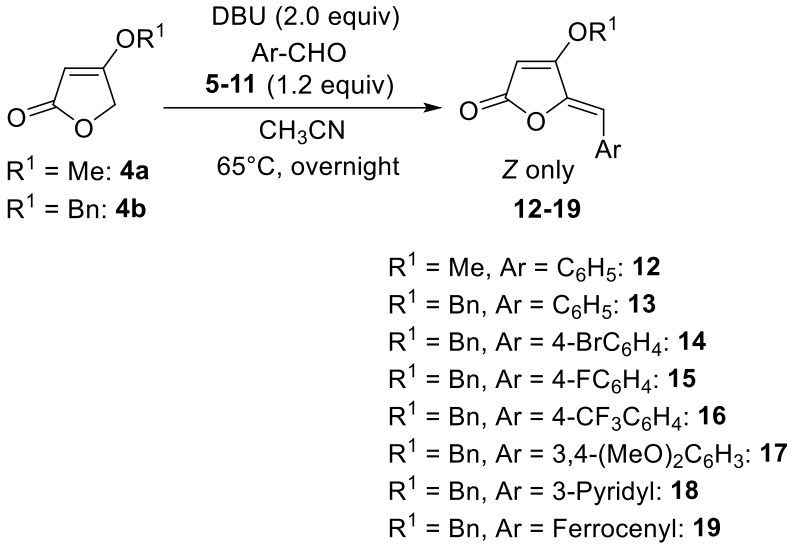

Scheme 1. General approach to prepare the γ-ylidene-tetronates **12-19** [12]

Lactones **12-19** were engaged in a Ring Opening-Ring Closure (RORC) lactamization reaction with a series of ferrocenyl alkyl amines [$Fc(CH_2)_nNH_2$; n = 1, 2, 3; Fc = Ferrocenyl] as well as with 4-trifluoromethylphenyl benzyl amine (for lactones **16** and **19**) (Table 1, scheme 2). The transformation was conducted in anhydrous MeOH, in a sealed tube at 80°C, until complete consumption of the starting γ-lactone (overnight). Corresponding γ-lactams **20-30** were obtained in moderate to good yields after evaporation of solvent and purification by silica gel chromatography. Structure of **24** was confirmed by single-crystal X-ray diffraction (Figure 3).

Table 1. Synthesis of ferrocenyl-containing γ-hydroxy-γ-lactams **20-28**

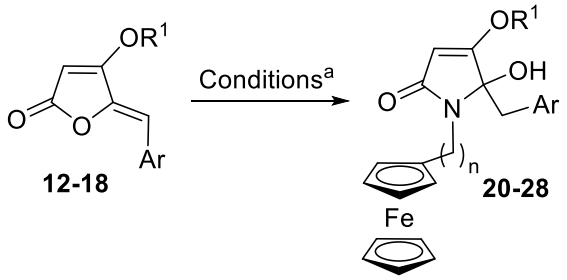

Entry	Starting material	R^1	Ar	n	Lactam (Yield, %)[b]
1	**12**	Me	Ph	1	**20** (69)
2	**13**	Bn	Ph	1	**21** (85)
3	**14**	Bn	4-BrC_6H_4	1	**22** (25)
4	**15**	Bn	4-FC_6H_4	1	**23** (25)
5	**16**	Bn	4-$CF_3C_6H_4$	1	**24** (55)
6	**17**	Bn	3,4-$(MeO)_2C_6H_3$	1	**25** (24)
7	**18**	Bn	3-Pyridyl	1	**26** (54)
8	**18**	Bn	4-$CF_3C_6H_4$	2	**27** (21)
9	**18**	Bn	4-$CF_3C_6H_4$	3	**28** (56)

[a]Reagents and conditions: $Fc(CH_2)_nNH_2$ (Fc: ferrocenyl, 1.2 equiv), MeOH, 80°C, overnight. [b]Isolated yield.

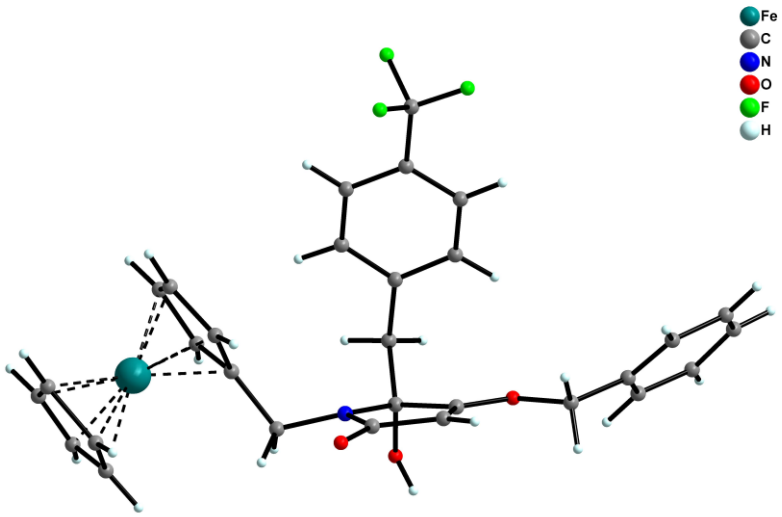

Figure 3. Single-crystal X-ray diffraction analysis of lactam **24**.

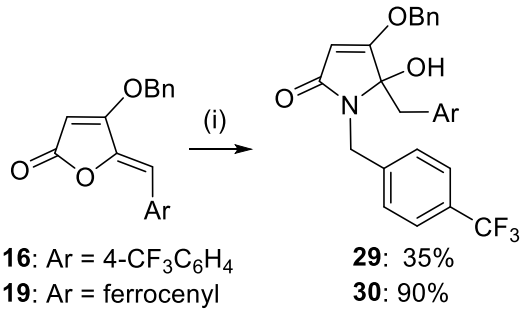

16: Ar = 4-$CF_3C_6H_4$
19: Ar = ferrocenyl

29: 35%
30: 90%

Scheme 2. Reagents and conditions: (i): 4-$CF_3C_6H_4CH_2NH_2$ (2 equiv), MeOH, 80 °C, overnight.

Post-modification of lactam **24** through the derivatization of the γ-hydroxy function was attempted to produce new ether-derived lactams **31**-**37** bearing pendant alkyl (**31**, **32**), ether (**33**), amine (**34**), ester (**35**) or nitrile (**36**) moieties (scheme 3). Lactams **31**-**34** were synthesized through the *in-situ* generation of iminium and reaction with appropriate alcohol (in excess), while lactams **35**-**36** were obtained by deprotonation of the hydroxyl function with NaH and alkylation with appropriate alkyl halides ($BrCH_2CO_2Et$, $ClCH_2CN$). Finally, ester-derived lactam **37** was readily obtained using acetic anhydride in the presence of catalytically amount of DMAP. Structures of **31** and **33** were confirmed by single-crystal X-ray diffraction (Figures 4-5).

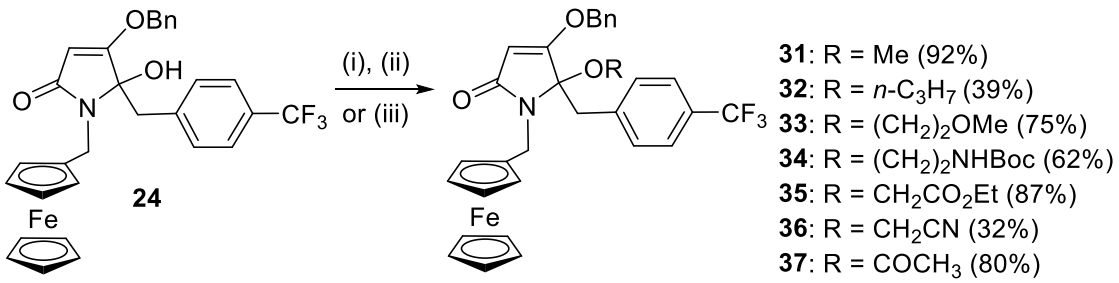

Scheme 3. Reagents and conditions: for **31**-**34**, (i): ROH (30 equiv), PTSA (0.1 equiv), CH_2Cl_2, 50-60 °C, 1-2 h; for **35**-**36**, (ii): 1) NaH (2 equiv), THF, 2) RX (5 equiv), r.t., 0.5-1 h; for **37**, (iii): Ac_2O (8 equiv), cat. DMAP, CH_2Cl_2, r.t., 30 min.

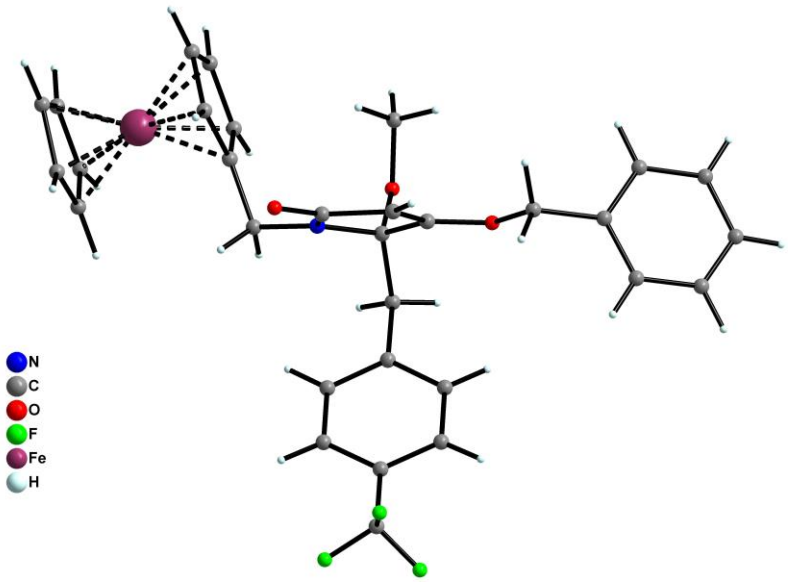

Figure 4. Single-crystal X-ray diffraction analysis of lactam **31**

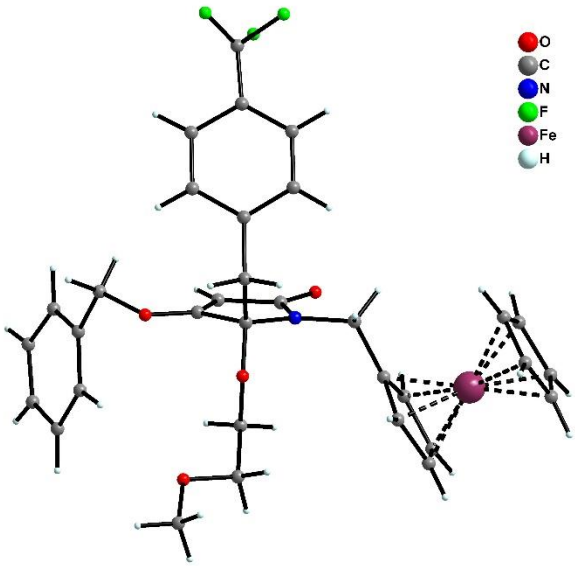

Figure 5. Single-crystal X-ray diffraction analysis of lactam **33**

2.2. Anti-plasmodial activities in vitro

Ferrocenyl-containing γ-tetramates **20-28** and derivatized-lactams **31-33, 35-37** were evaluated against CQ-sensitive (3D7) and CQ-resistant (W2) clones of *P. falciparum* (Tables 2-4) (Table S1, ESI) [8, 19]. All experiments were carried out twice in assays with drug concentrations in triplicate. Data are reported as IC_{50} values.

Table 2. *In vitro* data for compounds **20-28** against *P. falciparum* clones and resistance index.

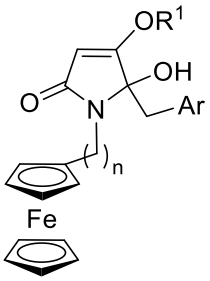

Compound	R^1	Ar	n	IC_{50} (3D7, nM)[a]	IC_{50} (W2, nM)[a]	RI[b]	cLogP[c]
20	Me	Ph	1	14591±1386	10793±565	0.80	2.85
21	Bn	Ph	1	1788±32	1088±80	0.61	4.34
22	Bn	4-BrC_6H_4	1	339±8	301±7	0.89	5.20
23	Bn	4-FC_6H_4	1	712±49	567±39	0.79	4.48
24	Bn	4-$CF_3C_6H_4$	1	90±8	112±22	1.25	5.22
25	Bn	3,4-$(MeO)_2C_6H_3$	1	214±15	175±12	0.82	4.00
26	Bn	3-Pyridyl	1	4938±177	2773±99	0.56	2.84
27	Bn	4-$CF_3C_6H_4$	2	>12800	>12800	/	5.83
28	Bn	4-$CF_3C_6H_4$	3	1066±337	781±39	0.74	6.21
CQ	/	/	/	30±3	750±18	25	

[a] Values are means determined from at least two experiments. Effective concentration for 50% inhibition; [b] Resistance index: RI = IC_{50}(W2)/IC_{50}(3D7); [c] clogP calculated from ChemDraw 19.0.

The derivatives are less active than chloroquine (**CQ**) on 3D7 strain; however, some of them are slightly more active on W2 strain (**22**, **24** and **25**) displaying promising mid-nanomolar activity with approximatively equal activity on both clones. **24** was identified as the best active in these series. When comparing methyl and benzyl tetramate (**20** *vs* **21**), the benzyl derivative is more active. It is suggested that the activity is probably due to the highest lipophilicity generated by the benzyl group. Regarding electronic effect on the Ar moiety, no clear conclusion can be drawn since either electron-withdrawing (**22**-**24**) or electron-donating substituents (**25**) induce good activity. The derivative having Ar = 3-pyridyl (**26**) is less active and that can be due to some chelation effects or other unknown factors. The distance between the ferrocene moiety and the lactam skeleton is critical to the activity since derivative **24** having one CH_2 is best active than derivatives **27** and **28** having two or three CH_2, with surprisingly **28** being at least 10 times more active than **27**. In order to understand if the activity of **24** was due

to its higher lipophilicity, compound **29** having a 4-trifluoromethylphenyl moiety in place of ferrocene was tested against 3D7 and W2 clones (Table 3). It appeared that **29** was less active [**29**: IC_{50} (3D7, nM) = 951; IC_{50} (W2, nM) = 1357] suggesting that lipophilicity is not the only factor. Position of the ferrocene moiety is also critical for activity since **30** [IC_{50} (3D7, nM) > 12 800; IC_{50} (W2, nM) > 12 800] is not active when compared to **24**. There are no define correlation of the cLogP parameter and antimalarial activity.

Table 3. *In vitro* data for compounds **29**-**30** against *P. falciparum* clones and resistance index

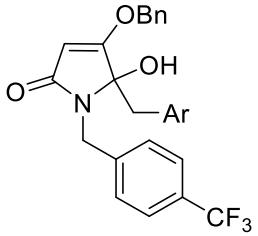

Compound	Ar	IC_{50} (3D7, nM)[a]	IC_{50} (W2, nM)[a]	RI[b]	cLogP[c]
29	4-$CF_3C_6H_4$	>800	>800	/	6.45
30	Ferrocenyl	>12800	>12800	/	5.21
CQ	/	30±3	750±18	25	

[a] Values are means determined from at least two experiments. Effective concentration for 50% inhibition; [b] Resistance index: RI = IC_{50}(W2)/IC_{50}(3D7);); [c] clogP calculated from ChemDraw 19.0.

Selected most active compounds (**22**, **24**, **25**) were evaluated against Human Umbilical Vein Endothelial Cells (HUVEC) using final concentrations ranging from 0.01 to 50 µM [19]. We did not detect significant cytotoxicity and no relevant CC_{50} could be obtained in the concentration range tested. Based on these data, we extrapolate a minimum cytotoxicity value over 10 to 50 µM for these compounds, leading to good selectivity against parasites (for both clones).

Table 4. *In vitro* data for compounds **31**-**37** against *P. falciparum* clones and resistance index.

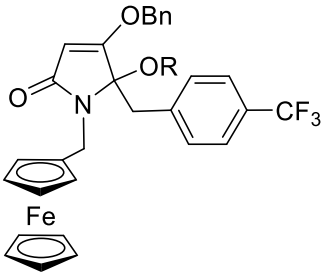

Compound	R	IC_{50} (3D7, nM)[a]	IC_{50} (W2, nM)[a]	RI[b]	clogP[c]
31	Me	518±26	374±18	0.72	5.78
32	*n*-C_3H_7	2209±20	1858±4	0.84	6.71
33	$(CH_2)_2OMe$	2156±65	1284±22	0.59	5.61
34	$(CH_2)_2NHBoc$	ND	ND	/	6.96
35	CH_2CO_2Et	1388±116	1026±32	0.74	6.18
36	CH_2CN	1564±233	1576±16	1.00	5.05
37	$COCH_3$	218±4	282±7	1.29	5.85
CQ	/	30±3	750±18	25	

[a] Values are means determined from at least two experiments. Effective concentration for 50% inhibition; [b] Resistance index: RI = IC_{50}(W2)/IC_{50}(3D7); N.D = not determined.; [c] clogP calculated from ChemDraw 19.0.

The derivatized-lactams **31-33, 35-37** were prepared either to see if the γ-hydroxy in the hemiaminal function is critical for the activity (**31-33**) or to access structures that could improve aqueous solubility, with also possible sites for further chemical elaboration (**35-37**). None of these hemiaminal-ether type lactams were potent as **24**, with the exception of **31** and **37**, suggesting that a naked -OH is critical for activity. Noteworthy to mention that **37** was found to produce **24** at pH ~ 5.4 (LC/MS) over 5h explaining its good activity.

2.3. Anti-plasmodial activities in vivo (mice)

The poor aqueous solubility of ferrocenyl-containing γ-tetramates **20-28** precluded their use via intra-peritoneal route in malaria-infected mice. **24** was then solubilized in peanut oil and administrated at increasing doses ranging from 5 to 50 mg/kg *per os* at day five post-malaria infection, once a day for three days. The disease worsening was clearly documented by a significant weight loss after the onset of symptoms for the untreated (negative control group) and treated groups (except artesunate control group). There was no significant decrease in blood

parasitemia during the treatment follow-up whatever the doses used. Artesunate treated group was cured as expected. No biological toxicity was observed during the treatment, according to haematological, renal and hepatic biomarkers.

2.4. Electrochemical studies

Electrochemical properties of selected ferrocenyl-containing γ-tetramates **22-26** were investigated using cyclic voltammetry in acetonitrile containing *n*-Bu_4NPF_6 as supporting electrolyte. Data obtained were compared with oxidation potentials of ferrocene and **FQ** [20] (Table 5).

Table 5. Oxidation potentials of lactams **22-26**[a]

Compound	$E_{1/2}$[b]	$E_{1/2}$[c]	IC_{50} (3D7, nM)	IC_{50} (W2, nM)
22	+ 0.089	+ 0.439	339±8	301±7
23	+ 0.074	+ 0.424	712±49	567±39
24	+ 0.095	+ 0.445	90±8	112±22
25	+ 0.098	+ 0.448	214±15	175±12
26	+ 0.083	+ 0.433	4938±177	2773±99
Ferrocene	+ 0.088	+ 0.438	/	/
FQ	/	+ 0.461[d]	7	13

[a] CH_3CN + 0.1 M *n*-Bu_4NPF_6; glassy carbon 3 mm; scan rate = 0.2 V s^{-1}; r. t.; [b] V *vs* Ag/Ag^+ 0.01M; [c] V *vs* SCE; [d] From reference [20].

All compounds exhibited single one-reversible oxidation wave (cyclic voltammograms are presented in ESI, Fig.S1) similar to ferrocene and ferroquine. From the data reported in table 5, there is insignificant change in the redox behavior of **22-26** since the ferrocene unit is insulated from the electronic effects of the aryl moiety. In addition, no clear correlation with the anti-plasmodial activity was observed.

2.5. Physico-biochemical studies

Capacity of the substrates to interact with hematin. In these experiments selected ferrocenyl-containing γ-tetramates (**22**, **24**, **25** and **26**), chloroquine-like tetramate **2** and references compounds **CQ** and **FQ** were studied. The affinity of our compounds for hematin Fe^{III}PPIX was first investigated by UV-visible absorption spectrophotometry under quasi-

physiological conditions (i.e. pH 7.5 that prevents hematin crystallization). Under these pH conditions, hematin predominantly exists as a π-π dimer [21]. The high-spin hematin possesses a spin of S = 5/2 with all half-filled d-orbitals in close proximity with the porphyrin HOMO and LUMO. This results in a strong overlap between the porphyrin π-π* (eg π* excited state orbitals) and the Fe^{III} d transitions (dyz, dxz orbitals). This is reflected by broad Q bands in the visible absorption region (Figure 6). Similarly to ferric high spin derivatives (e.g. myoglobin, hemoglobin), a characteristic charge transfer CT band (i.e. band III, a2u → dyz) centered at ~ 610 nm can be also observed. Last but not least, exciton transfer occurs within the hematin π-π dimer from electronic interaction (i.e. electron exchange between the individual chromophores) by direct overlap of the π orbitals of the porphyrins (i.e. face to face arrangement). This exciton interaction in the ground state breaks the degeneracy of the B (or Soret absorption band) excited state, giving rise to two Soret bands lying at 383 nm and 364 nm, respectively (Figure 6). This broad and split Soret band is thus as a clear and valuable spectroscopic signature of the occurrence of the hematin π-π dimer in solution (K_{Dim} = $10^{6.8}$ M^{-1} at pH ~ 7.5).

Upon addition of the substrates containing a quinolone skeleton (**CQ**, **FQ** and **2**), concomitant bathochromic shifts and narrowing of the broad and split Soret band is observed for all these substrates (Figures 6 and 7), thus emphasizing the formation of stable complexes with the hematin π-π dimer (i.e. the stoichiometry substrate/hematin π-π dimer 1/1 was already evidenced for **CQ** [22] and is supported in this work by Job plot experiments, Figure S2, ESI).

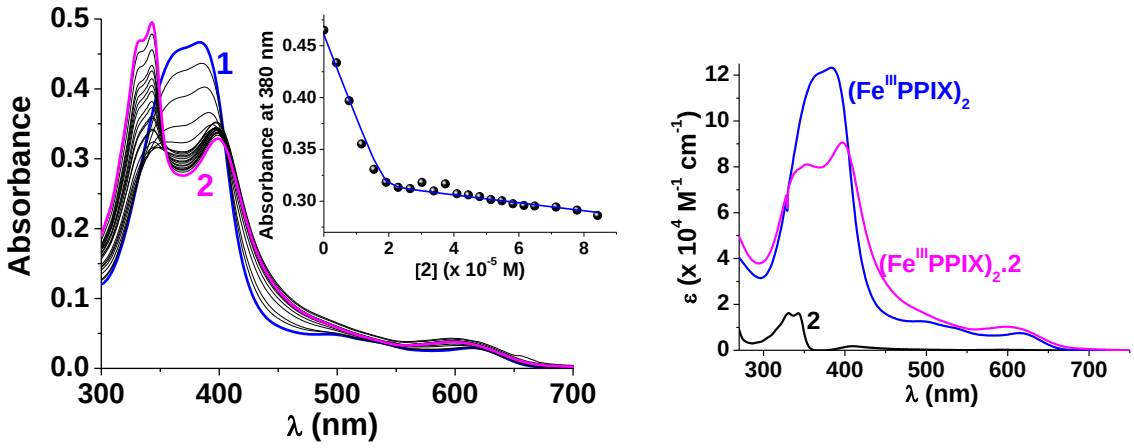

Figure 6. (left) Spectrophotometric titration of hematin **Fe^{III}PPIX** (under its π-π dimeric form, log K_{Dim} = 6.82) by **2** (inset: variation of the absorbance at 380 nm as a function of the substrate concentration). (right) Electronic spectra of hematin, the free **2** substrate and their corresponding Fe^{III}PPIX.substrate complexes. Solvent: 0.2 M aqueous sodium HEPES buffer

pH 7.5; T = 25.0 °C; l = 1 cm. [**Fe^{III}PPIX**]$_0$ = 3.92 × 10^{-5} M; (1) [**2**]$_0$/[**Fe^{III}PPIX**]$_0$ = 0; (2) [**2**]$_0$/[**Fe^{III}PPIX**]$_0$ = 2.4.

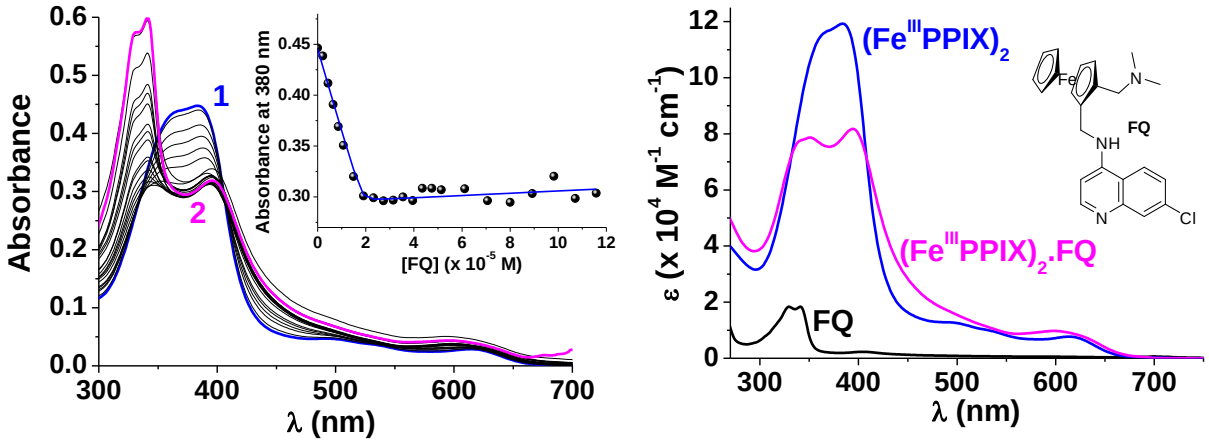

Figure 7. (left) Spectrophotometric titration of hematin **Fe^{III}PPIX** (under its π-π dimeric form, log K_{Dim} = 6.82) by **FQ** (inset: variation of the absorbance at 380 nm as a function of the substrate concentration). (right) Electronic spectra of hematin, the free **FQ** substrate and their corresponding Fe^{III}PPIX.substrate complexes. Solvent: 0.2 M aqueous sodium HEPES buffer pH 7.5; T = 25.0 °C; l = 1 cm. [**Fe^{III}PPIX**]$_0$ = 3.92 × 10^{-5} M; (1) [**FQ**]$_0$/[**Fe^{III}PPIX**]$_0$ = 0; (2) [**FQ**]$_0$/[**Fe^{III}PPIX**]$_0$ = 2.40.

For **22**, **24**, and **25**, the lack of quinoline subunit enlightens the failure of these substrates to interact efficiently with the hematin π-π dimer (i.e. no hematin complexes with **22**, **24** and **25** were evidenced, Figure 8 and Figures S3-S5, ESI).

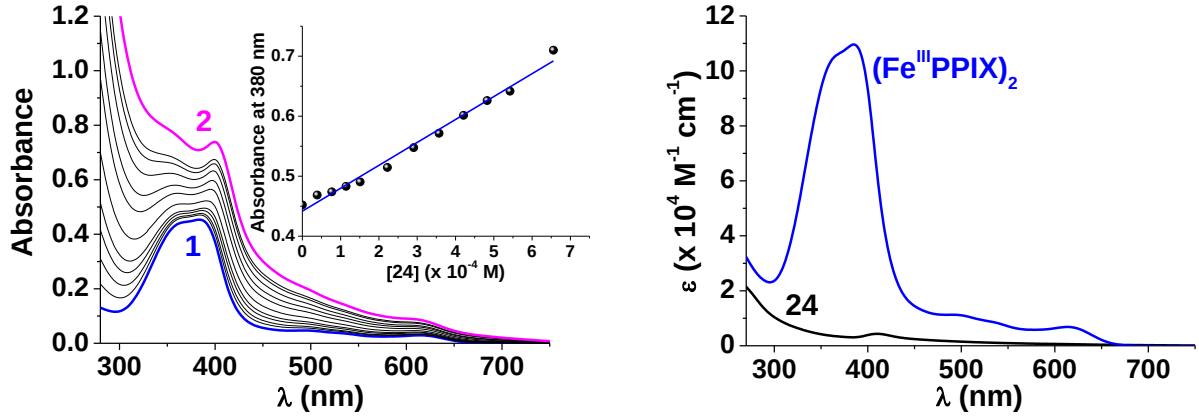

Figure 8. (left) Spectrophotometric titration of hematin **Fe^{III}PPIX** (under its π-π dimeric form,

log K_{Dim} = 6.82) by **24** (inset: variation of the absorbance at 380 nm as a function of the substrate concentration) showing the absence of interaction between the hematin π-π dimer and **24**. (right) Electronic spectra of hematin and the free **24** substrate. Solvent: 0.2 M aqueous sodium HEPES buffer pH 7.5; T = 25.0 °C; l = 1 cm. [**Fe^{III}PPIX**]$_0$ = 3.92 × 10^{-5} M; (1) [**24**]$_0$/[**Fe^{III}PPIX**]$_0$ = 0; (2) [**24**]$_0$/[**Fe^{III}PPIX**]0 = 20.0.

The association constants K_A (M^{-1}), the dissociation constants K_D (μM) and the stoichiometries of the species at equilibrium have been determined by processing the spectrophotometric data (Table 6). The comparable K_D values (i.e. in the micromolar range) and spectral characteristics indicated similar interactions of the quinoline-based substrates (**CQ**, **FQ** and **2**) with the hematin π-π dimer. On the other hand, it has been reported that the binding of methylene blue (**MB**), an antiparasitic substrate acting as a "redox cycler", also induces a significant narrowing and red shift of the Soret band of the hematin π-π dimer. This spectroscopic finding (loss of exciton coupling) suggested intercalation of **MB** between the two Fe^{III}PPIX in a sandwich-type structure [23]. Similar arrangement can be thus be proposed for the quinoline-based substrates as shown by the narrowing and bathochromic shift of the broad and split B band of the hematin π-π dimer upon interactions with the quinoline moieties of **CQ**, **FQ** and **2**.

Table 6. Binding properties of the substrates considered in this work with the hematin π-π dimer.[a]

	Interaction with hematin π-π dimer			β-Hematin inhibition[b]
Stoichiometry	Stability constant log $\beta_{(FePPIX)2}$-s (± σ)	log K_A (M^{-1})[c]	K_D (μM)	IC_{50} (max. inhibition reached (%) at drug:hematin ratio)
FQ + 2Heme	12.2 ± 0.4	5.38	4.16	0.3 [76 (0.75:1)]* 0.4 [86% (0.75:1)]*
2 + 2Heme	13.2 ± 0.2	6.38	0.42	nd
CQ + 2Heme **CQ** + 2Heme 2**CQ** + Heme	12.7 ± 0.2 [25] 13.17 ± 0.07	5.88 6.35 5.51[e,f] [26]	1.30 0.45 3.09	1.9 [89% (3:1)] [24] 1.60 [86% (2:1)] [22]

2**CQ** + Heme		6.06[d,f] [26]	0.87	
22 + Heme	ni	na	na	na
24 + Heme	ni	na	na	na
25 + Heme	ni	na	na	na

[a] Solvent: 0.2 M aqueous sodium HEPES buffer pH 7.5; T = 25.0 °C; [b]12.9 M sodium acetate buffer pH 4.5, 60 °C, 1 h then 0.2 + 0.02 M sodium HEPES buffer pH 7.5 containing 5% pyridine (v/v) as reporting reagent; see refs. [21, 22]. [c]log K_{Dim} = 6.82 [23]; [d]pH 7.43-7.5. [e]pH 5.6. [f]Interactions with hemin chloride. ni = no interaction. nd = not determined. na = not applicable. *: a bell-shaped curve was observed [24]. K_A = association constant (M^{-1}). K_D = $1/K_A$ = dissociation constant (µM). β-Hematin = synthetic hemozoin.

Furthermore, the absence of the lysosomotropic quinoline unit for **22**, **24-26** (i.e. that is concentrated in its protonated state in acidic organelles due to proton trapping) disables the trafficking of these substrates within the acidic food vacuole (FV) where hemoglobin digestion by the parasite occurs and where subsequent biocrystallisation of the prosthetic hematin into hemozoin takes place. As a consequence, **22**, **24-26** likely do not prevent hemozoin formation in the FV but rather act as Fenton catalysts in the cytosol (see below) supporting their antimalarial activity. Some precedents in literature [20] have shown that **FQ**, which possesses both a 4-aminoquinoline ring and a ferrocenyl moiety in its amino-side chain, is able to generate hydroxyl radicals from H_2O_2 via a Fenton-like reaction. In the following investigation, the capacity of all ferrocene-based derivatives (**22**, **24-26**) to act as Fenton catalysts was evaluated in comparison to that of **FQ**. The objective was to break down the contribution of the Fenton catalysis versus hematin binding and hemozoin inhibition at the origin of the antimalarial processes of the ferrocenyl-based agents.

Oxidation with Fenton's reagent based on a ferrous (or ferrocene) redox active core and H_2O_2 has been proven to be an efficient route to decompose a wide range of organic dyes. The hydroxyl radical $^{\bullet}OH$ (i.e. that reacts in a diffusion-controlled manner with second-order rate constant in the range of 10^9–10^{10} M^{-1} s^{-1}) is the main product of that process that is capable of degrading a large number of organic substrates via unselective oxidation. For example, upon reaction with $^{\bullet}OH$, the colour of the **MB** chromophore irreversibly vanished as the consequence of its degradation through simultaneous pathways that forms, among others, chloride, nitrate and sulfate, as well as low molecular weight intermediates such as benzothiazoles, phenol, and

hydroxyl or sulfonate derivatives of **MB** [27]. We have therefore taken advantage of this property to evaluate the capacity of our substrates to act as efficient Fenton catalysts. The kinetics of activation of the Fenton catalysts was assessed indirectly by monitoring spectrophotometrically the fading process of **MB**. Figure 9 first depicts the spectral variation recorded during the reaction with ferrocene (**Fc**) or **25**, as well as the kinetics parameters that were calculated. Invariantly, the absorption band of **MB** centred at 660 nm decreases as a function of time in an exponential manner, suggesting that the whole process (i.e. activation of the Fenton catalyst/fading reaction of **MB**) is controlled by a single rate-determining step. From the calculated data, it was shown (i.e. irrespective of the catalyst used, it is expected that the fading kinetics of **MB** is the same) that the fading reaction of **MB** is fast with respect to the Fenton reaction, thus demonstrating the significance of this assay to reflect the reactivity of the Fe(II)-containing catalysts to trigger a Fenton process. Table 7 gathers the apparent rate constants (k_{obs}, min^{-1}) that were estimated for the catalysts considered in this work, as well as the corresponding half-time values (min). Ferrocene (**Fc**) and free ferrous ion **Fe(II)** were found to be among the most efficient H_2O_2 activators within the series of compounds examined.

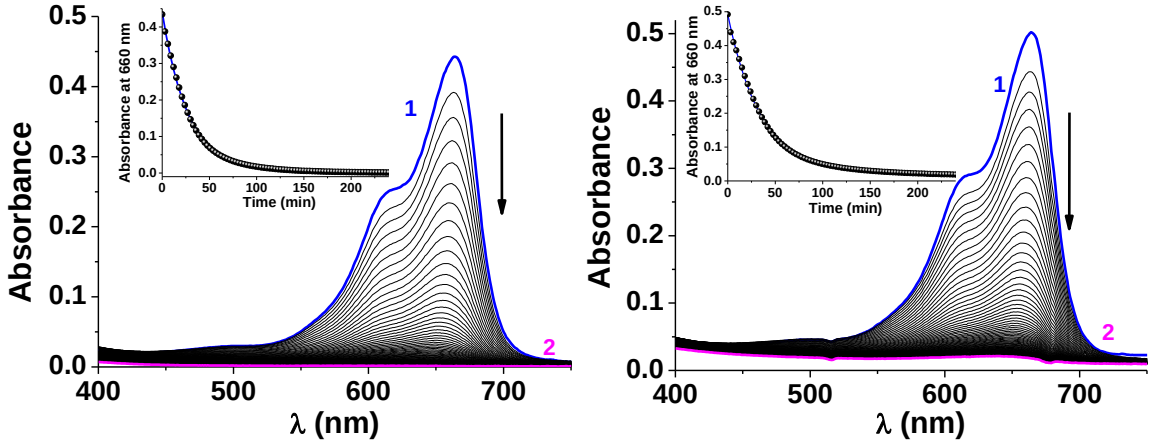

Figure 9. Visible absorption spectral variation centred on **MB** along the Fenton reaction catalyzed by (left) **Fc** and (right) **25** in aqueous solution. (insets: variation of the absorbance at 660 nm as a function of time). Solvent: water at pH 3; T = 37.0 °C; l = 0.2 cm. $[\mathbf{MB}]_0 = 3 \times 10^{-5}$ M; $[\mathbf{Fc}]_0 = [\mathbf{25}]_0 = 9.5 \times 10^{-5}$ M; $[H_2O_2]_0 = 3.26 \times 10^{-2}$ M.

Table 7. Kinetic parameters of the substrates considered in this work in the Fenton reaction probed by monitoring the fading of the **MB** dye.

Substrate/Catalyst	k_{obs} (10^{-2} min^{-1})	$t_{1/2}$ (min)
Fe^{II}	1.90	36

Fc	3.38	21
FQ	pb	na
2	nr	na
24	1.13	61
25 (pH 3)	2.69	26
25 (pH 7)	slow reaction	na
22	0.91	73
26	1.06	65

Solvent: water at pH 3; T =37°C; [**MB**]$_0$ = 3 × 10^{-5} M; [Fc]$_0$ = [**Substrate**]$_0$ = 9.5 × 10^{-5} M; [H_2O_2]$_0$ = 3.26 × 10^{-2} M. nr = no reaction; na = not applicable; pb = particular behaviour.

We have confirmed that the medium acidity plays a critical role in triggering the Fenton reaction. The reaction is indeed significantly slowed down when **25** is used as the iron(II) catalyst at pH 7, while the reaction is faster at pH 3 (Figure S6, ESI) in agreement with literature data [28]. The crucial role of the **Fc** activating unit was shown by comparing the reactivity of **24** (i.e. that contains a ferrocenyl unit) to that of **2** (i.e. that lacks a ferrocenyl unit). No fading reaction of **MB** occurs with **2** and excess of H_2O_2 thus demonstrating the critical role of the metal catalyst (Figure S7, ESI).

At pH 3, **25** displays a reactivity comparable to that of **Fc**, while **24**, **26** and **22**, which mainly differ from the substitution pattern on the benzyl unit of the γ-lactam, are less reactive (Table 7). It is unlikely that the substitution pattern of the lactam subunit (i.e. the ferrocenyl subunit is kept unchanged whatever the system considered) modulates the redox properties of the ferrocenyl electroactive core (see Table 5). We have indeed demonstrated insignificant change in the redox behavior of **22-26** by cyclic voltammetry (see above). The peculiar properties of **22**, **26** and **24** (Figure 10, Figures S7, S8), that contained electro-withdrawing (Br, CF_3) substituents or a pyridinyl moiety, might therefore be explained by the unselective reactivity of the hydroxyl radical •OH that is able to target the lactam unit as well in addition to the **MB** dye. The lesser reactivity of **22**, **24** and **26** can therefore be attributed to the weakness of the lactam residues, while the presence of electrodonating units for **25** likely stabilizes the lactam unit toward scavenging by •OH. As a consequence, the **Fc** unit borne by **25** is almost as effective as free Fc (Figure 11).

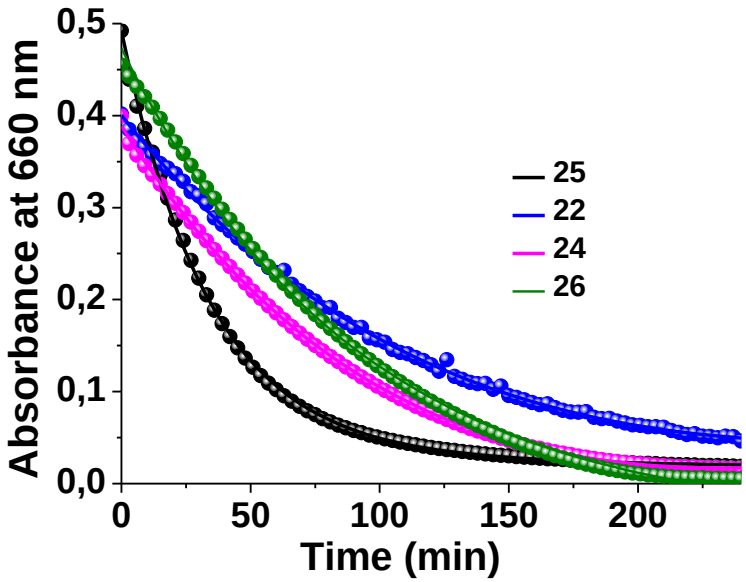

Figure 10. Variation of the absorbance at 660 nm centred on **MB** as a function of time for the Fenton reaction catalyzed by **25**, **22**, **26** or **24** in aqueous solution. Solvent: water at pH 3; T = 37.0 °C; l = 0.2 cm. [**MB**]$_0$ = 3 × 10^{-5} M; [**22**]$_0$ = [**25**]$_0$ = [**24**]$_0$ = [**26**]$_0$ = 9.5 × 10^{-5} M; [H_2O_2]$_0$ = 3.26 × 10^{-2} M.

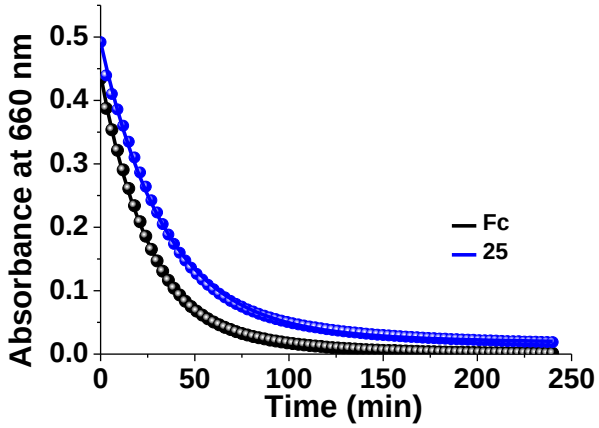

Figure 11. Variation of the absorbance at 660 nm as a function of time measured for **25** and **Fc** at pH 3. Solvent: water at pH 3; T = 37.0 °C; l = 0.2 cm. [**MB**]$_0$ = 3 × 10^{-5} M; [Fc]$_0$ = [**25**]$_0$ = 9.5 × 10^{-5} M; [H_2O_2]$_0$ = 3.26 × 10^{-2} M.

Further insight into this peculiar behaviour was obtained by comparing **Fc** with ferroquine (**FQ**), an antimalarial drug containing both a ferrocenyl and a 4-aminoquinoline unit that was shown (e.g. **CQ**) to be accumulated in the FV of the parasite cell and inhibit hemozoin formation. Furthermore, the stability of **FQ** was investigated in oxidizing conditions mimicking

the parasite's FV (acidic pH and micromolar concentrations in H_2O_2) [14]. The study performed by MALDI-TOF mass spectrometry clearly evidence the molecular degradation of **FQ** in water in the presence of H_2O_2 [20]. However, while this local production of hydroxyl radicals could not be sufficient to affect the stability of **FQ** at high rate in vivo, it has been proposed to allow the destruction of hematin itself, in agreement with the apparent slow decrease of inhibition of β-hematin formation observed in the presence of **FQ** (soft bell-shaped curve) at increasing **FQ**:hematin ratio [24].

Interestingly, **FQ** herein displayed a peculiar behaviour in the Fenton assay with a significant lag phase of about an hour with weak **MB** fading then followed by a much faster degradation of the dye (Figure 11). This would support the fact that the hydroxy radicals •OH generated by the ferrocenyl unit borne by **FQ** target more efficiently the quinoline moiety of **FQ** than **MB**, thus contributing to the formation of a lag phase prior to **MB** degradation [20]. To support this hypothesis, the same experiment has been carried out by using Fc and chloroquine (**CQ**) in the presence of H_2O_2 and **MB** at pH 3. Under these conditions (i.e. **Fc** has been clearly shown to efficiently activate H_2O_2, Figure 9), **MB** degradation is significantly inhibited over the timescale examined most likely by more efficient reaction with the exogenous **CQ** substrate. This supports the idea that the quinoline (**FQ**) or γ-lactam (**22**, **24**) that are linked to the ferrocenyl electroactive unit might influence the Fenton reaction by scavenging the hydroxyl radicals that are generated.

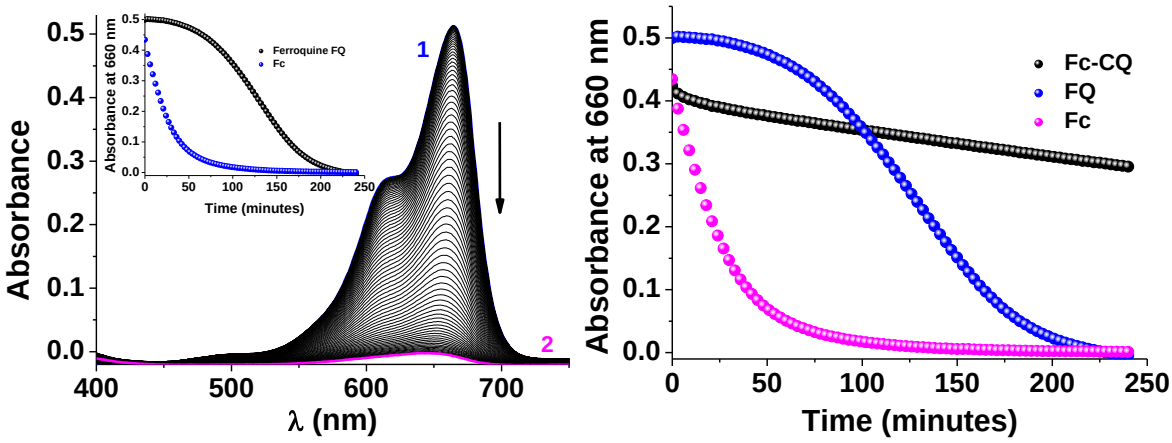

Figure 12. (left) Visible absorption spectral variation centred on **MB** along the Fenton reaction catalyzed by **FQ** in aqueous solution. (inset: variation of the absorbance at 660 nm as a function of time for **FQ** compared to **Fc**). (right) variation of the absorbance at 660 nm (absorption of **MB**) as a function of time for **FQ** compared to Fc and an equimolar mixture of **Fc** and **CQ**.

Solvent: water at pH 3; T = 37.0 °C; l = 0.2 cm. [**MB**]$_0$ = 3 × 10^{-5} M; [**Fc**]$_0$ = [**FQ**]$_0$ = [**CQ**]$_0$ = 9.5 × 10^{-5} M; [H_2O_2]$_0$ = 3.26 × 10^{-2} M.

It has been shown that, like chloroquine, ferroquine concentrates in the FV of CQ-sensitive parasite and targets the hematin detoxification [29]. However, the introduction of the ferrocene core in the lateral side chain of **CQ** has an important consequence: in **CQ**-resistant parasites the chloroquine resistance transporter *P*fCRT responsible for **CQ** efflux from the FV and loss of **CQ** efficacy is unable to efflux **FQ** from the FV [30, 31]. Once in the FV, the acidity of the medium (pH 5) as well as the presence of H_2O_2 (µM) triggers the Fenton reaction that contributes to the global antimalarial activity of **FQ**. **FQ** likely contributes to the Fenton-mediated degradation of the drug as demonstrated in this study, explaining the observed decrease of the hematin:drug ratio at pH 5.2 in the reporter assay with pyridine [32]. It has been indeed shown by ES-MS tools that oxidized/degradation products of **FQ** (quinoline oxide, loss of dimethylamino group) are slowly formed in oxidizing conditions mimicking the parasite FV. The use of more acidic conditions has a clear impact on the kinetics of **FQ** degradation as shown in this study. With respect to the γ-lactam derivatives that bear a ferrocenyl unit, it is unlikely that accumulation occurs in the FV. Therefore, it is anticipated that these ferrocene-based derivatives (**24**, **25**, **22**) are mainly localized in the cytosol of the parasitized red blood cells at neutral pH where they likely exert their antimalarial action *per se* in a distinct mechanism shown by **FQ**. Furthermore, the γ-lactam-ferrocenyl derivatives are unable to interact with hematin thus discarding a CQ-like activity. Even though these derivatives are by far less active than **CQ**, **FQ** or **2** (compounds that target the food vacuole), they display good antimalarial activities either on CQ^S or CQ^R parasites. Their mode of action might be related to their capacities to catalyze reactive oxygen species in a Fenton reaction in the cytosol at pH about 7. While Fenton reaction products and kinetics of oxidation of various substrates strongly support $^{\bullet}$OH radical formation in acidic media, the exact nature of other intermediate(s) - likely Fe(IV) species - generated at higher, near-neutral pH has been postulated for decades and deciphered recently [28].

3. Conclusion

A series of ferrocenyl-containing γ-hydroxy-γ-lactam tetramates was prepared in 2-3 steps and some representatives displayed promising *in-vitro* antiplasmodial activities, with **24** identified as the best active derivative. There is no correlation of the redox properties of these ferrocene

derivatives with their antimalarial activities. Our work evidenced for the first time that new ferrocene-based derivatives can exert potent antimalarial activities *via* a mechanism distinct from that of **FQ**. Their reactivity toward a Fenton reaction is proposed to be dependent on both their specific ferrocene-based C-Mannich base structures functionalized with an original hydroxyl-lactam motif and the physico-chemical conditions of their environment at the pH of the cytosol of *P. falciparum* parasites. Generally, the ferrocenyl-derived tetramates are characterized by a poor aqueous solubility prohibiting then *in vivo* studies on a mouse model by a *i.p* route. Compound **24** was then solubilized in peanut oil and administrated orally at 5-50 mg/kg *per os*. However, no significant decrease of parasitemia and no biological toxicity was observed. The reasons why compound **24** failed to exert *in vivo* activity remain unclear, however its poor solubility is a major issue. In addition, it will definitely help to know the catabolism pathway(s) of **24**. Optimization of the pharmacokinetics properties of **24** should be programmed in order to validate if these ferrocenyl-containing γ-hydroxy-γ-lactam tetramates deserve further interest as potent antimalarials.

4. Experimental

4.1. Chemistry

4.1.1. General

Solvents were of highest purity and anhydrous and were purchased from Acros Organics and Sigma Aldrich. Reagents were obtained commercially (Acros Organics, Sigma Aldrich) and used without further purification. Lactones **12**-**19** were synthesized as described in reference [10]. Ferrocenyl alkylamines $Fc(CH_2)_nNH_2$ were synthesized according to published procedures ($Fc(CH_2)_nNH_2$; n = 1 [33], 2 [34], 3 [35]). ^1H, ^{19}F and ^{13}C NMR spectra were recorded with a Bruker Avance 300 or a DRX300 spectrometer ($CDCl_3$ or CD_3OD) at 300 MHz, 282 MHz and 75 MHz, respectively. Chemical shifts are given in parts per million (ppm) relative to residual peak of solvent or external $CFCl_3$ (^{19}F). The following abbreviations are used to describe peak patterns: s (singlet), d (doublet), t (triplet), m (multiplet), q (quadruplet) and br (broad). Coupling constants are given in Hertz. High-resolution mass spectra (HRMS) were recorded using a MicroTOF-Q II (electrospray ionization (ESI) mode). The purities of compounds selected for in vitro and in vivo antiplasmodial studies were ≥ 95%, measured by UPLC/MS, which were performed on an Thermo Fisher Scientific U300 HPLC system connected to a Bruker MicroTOF-Q II (Bremen, Germany) mass spectrometer. Separations were carried out on Luna Omega C18 column (10 cm x 2.1 cm; 1.6 µm) with a flow rate of 0.4 mL/min at 40°C. Two mobile phases [mobile phase A 100% water with 0.1% of formic acid;

mobile phase B methanol/acetonitrile (50:50) with 0,1% formic acid] were employed to run a gradient condition from 100% A to 100% B in 20 minutes hold for 5 minutes and back to initial conditions in 5 minutes, hold for 5 minutes. An injection volume of 1 µL was used. The mass spectra were acquired by scanning from 50 to 1000 uma in the positive ion mode with a spray voltage of 5 kV. The calibration of the mass spectrometer was performed by using formiate buffer, the measured mass precision is less than 5 ppm. Samples were prepared by mixing 10 µL of 1mg/mL of compound in methanol in 1 mL of water. Thin-layer chromatography (TLC) was performed on silica gel GF254 plates. Macherey-Nagel Silica gel 60M (0.04-0.063 mm) was used for silica gel chromatography. Melting points (uncorrected) were determined in capillary tubes on a Büchi apparatus.

*4.1.2. Synthesis of lactams **20-30***

Typical procedure for the preparation of γ-lactams (**20**-**28**). To a solution of lactone **16** (0.40 g, 1.16 mmol) in anhydrous MeOH (7.7 mL) was added (aminomethyl)ferrocene $FcCH_2NH_2$ (0.30 g, 1.39 mmol). Reaction mixture was then vigorously stirred at 80°C in a sealed tube overnight. Solvent was then evaporated in vacuo and residue was purified by silica gel column chromatography (eluent: petroleum ether/AcOEt, 1:1) giving 0.36 g (yield: 55%) of lactam **24** as a yellow solid.

*4.1.2.1.4-Methoxy-5-hydroxy-1-ferrocenemethyl-5-benzyl-1H-pyrrol-2(5H)-on***e 20.**

Yield: 69% (0.29 g); yellow solid; mp 194-195 °C. ^{1}H NMR (CD_3OD, 300 MHz): δ 7.12-7.07 (m, 3H), 6.88-6.84 (m, 2H), 4.64 (s, 1H), 4.46-4.30 (m, 4H), 4.21 (s, 5H), 4.17-4.13 (m, 2H), 3.70 (s, 3H),), 3.22 (d, J = 13.5, 1H), 3.02 (d, J = 13.5, 1H). ^{13}C NMR (CD_3OD, 75 MHz): δ 177.0, 173.1, 136.1, 131.2, 129.1, 128.1, 94.0, 91.9, 72.1, 72.0, 69.9, 69.7, 69.2, 58.9, 41.7, 39.0. HRMS (ESI^+): *m/z* calcd. for $[M + Na]^+$ $C_{23}H_{23}FeNNaO_3$ 440.0920, found 440.0909.

4.1.2.2. 4-Benzyloxy-5-hydroxy-1-(ferrocenemethyl)-5-benzyl-1H-pyrrol-2(5H)-one **21.**

Yield: 85% (0.42 g); yellow solid; mp 151 °C. NMR: not possible due to low solubility. HRMS (ESI^+): *m/z* calcd. for $[M + H]^+$ $C_{29}H_{28}FeNO_3$ 493.1339, found 493.1288.

4.1.2.3. 4-Benzyloxy-5-(4-bromobenzyl)-5-hydroxy-1-(ferrocenylmethyl)-1H-pyrrol-2(5H)-one **22**.

Yield: 25% (68 mg); beige solid; mp 203 °C. ^{1}H NMR ($CDCl_3$, 300 MHz): δ 7.40-7.38 (m, 3H), 7.31-7.23 (m, 4H), 6.76 (d, J = 8.1, 2H), 4.79 (d, J = 11.7, 1H), 4.72 (s, 1H), 4.71 (d, J = 11.4,

1H), 4.53 (d, *J* = 14.7, 1H), 4.40 (br s, 1H), 4.36 (br s, 1H), 4.24 (d, *J* = 15.0, 1H), 4.19 (s, 5H), 4.11 (br s, 2H), 3.18 (d, *J* = 13.8, 1H), 3.07 (d, *J* = 13.8, 1H), 2.72 (s, 1H). ^{13}C NMR ($CDCl_3$, 75 MHz): δ 172.3, 169.6, 134.2, 133.2, 131.4, 131.2, 128.9, 128.8, 128.0, 121.1, 94.5, 90.1, 84.6, 73.0, 70.4, 70.1, 68.7, 68.4, 39.4, 37.5. HRMS (ESI$^+$): *m/z* calcd. for $[M + H]^+$ $C_{29}H_{27}BrFeNO_3$ 571.0442, found 571.0435.

4.1.2.4. 4-Benzyloxy-5-(4-fluorobenzyl)-5-hydroxy-1-(ferrocenylmethyl)-1H-pyrrol-2(5H)-one **23**.

Yield: 25% (69 mg); yellow solid; mp 181 °C. ^{1}H NMR ($CDCl_3$, 300 MHz): δ 7.40-7.36 (m, 3H), 7.33-7.29 (m, 2H), 6.88-6.78 (m, 4H), 4.78 (d, *J* = 11.7, 1H), 4.700 (d, *J* = 11.4, 1H), 4.698 (s, 1H), 4.54 (d, *J* = 15.0, 1H), 4.40 (br d, *J* = 1.2, 1H), 4.36 (br d, *J* = 1.2, 1H), 4.24 (d, *J* = 15.0, 1H), 4.19 (s, 5H), 4.11 (br d, *J* = 1.2, 2H), 3.20 (d, *J* = 13.8, 1H), 3.09 (d, *J* = 14.1, 1H), 2.85 (s, 1H). ^{13}C NMR ($CDCl_3$, 75 MHz): δ 172.5, 169.7, 161.9 (d, *J* = 244.0), 134.3, 131.2 (d, *J* = 8.0), 129.9 (d, *J* = 3.2), 128.8, 128.7, 128.0, 114.9 (d, *J* = 21.0), 94.4, 90.3, 84.6, 73.0, 70.4, 70.1, 68.6, 68.3, 39.1, 37.5. ^{19}F NMR ($CDCl_3$, 282 MHz): δ -115.5 (m). HRMS (ESI$^+$): *m/z* calcd. for $[M + H]^+$ $C_{29}H_{27}FFeNO_3$ 511.1241, found 511.1223.

4.1.2.5. 4-Benzyloxy-5-hydroxy-1-(ferrocenylmethyl)-5-(4-trifluoromethylbenzyl)-1H-pyrrol-2(5H)-one **24.**

Yield: 55% (0.36 g); yellow solid; mp 192 °C. ^{1}H NMR ($CDCl_3$, 300 MHz): δ 7.38 (s, 5H), 7.27 (d, *J* = 7.5, 2H), 6.99 (d, *J* = 7.5, 2H), 4.79 (d, *J* = 11.7, 1H), 4.71-4.69 (m, 2H), 4.51 (d, *J* = 14.7, 1H), 4.39 (s, 2H), 4.30 (d, *J* = 15.0, 1H), 4.19 (s, 5H), 4.13-4.11 (m, 2H), 3.27 (d, *J* = 13.8, 1H), 3.18 (d, *J* = 13.8, 1H), 2.98 (br s, 1H). ^{13}C NMR ($CDCl_3$, 75 MHz): δ 172.4, 169.8, 138.3, 134.2, 130.1, 129.1 (q, *J* = 35.3), 128.9, 128.7, 127.9, 124.8 (q, *J* = 3.8), 124.1 (q, *J* = 270.5), 94.3, 89.9, 84.5, 73.0, 70.4, 70.2, 68.6, 68.4, 68.2, 40.0, 37.5. ^{19}F NMR ($CDCl_3$, 282 MHz): δ -62.5 (s). HRMS (ESI$^+$): *m/z* calcd. for $[M + H]^+$ $C_{30}H_{27}F_3FeNO_3$ 561.1209, found 561.1198.

4.1.2.6. 4-Benzyloxy-5-(3,4-dimethoxybenzyl)-5-hydroxy-1-(ferrocenylmethyl)-1H-pyrrol-2(5H)-one **25.**

Yield: 24% (0.12 g); yellow solid; mp 153 °C. ^{1}H NMR (CD_3OD, 300 MHz): δ 7.40-7.37 (m, 5H), 6.67 (d, *J* = 8.4, 1H), 6.46 (dd, *J* = 8.1, 1.5, 1H), 6.37 (d, *J* = 1.5, 1H), 4.89 (d, *J* = 12.0, 1H), 4.78 (s, 1H), 4.75 (d, *J* = 12.0, 1H), 4.51 (d, *J* = 15.0, 1H), 4.50 (br s, 1H), 4.40 (br s, 1H),

4.31 (d, *J* = 14.7, 1H), 4.21 (br s, 5H), 4.17 (br s, 1H), 4.14 (br s, 1H), 3.73 (s, 3H), 3.53 (s, 3H), 3.23 (d, *J* = 13.8, 1H), 2.97 (d, *J* = 13.5, 1H). ^{13}C NMR (CD_3OD, 75 MHz): *δ* 175.9, 173.3, 149.8, 149.4, 136.5, 129.7, 129.6, 129.1, 128.7, 123.8, 114.5, 112.3, 94.6, 91.8, 85.7, 74.1, 72.1, 71.8, 69.7, 69.6, 69.0, 56.8, 56.4, 41.1, 38.7. HRMS (ESI^+): *m/z* calcd. for $[M + H]^+$ $C_{31}H_{32}FeNO_5$ 553.1546, found 553.1538.

4.1.2.7. 4-Benzyloxy-5-hydroxy-1-(ferrocenylmethyl)-5-(pyridin-3-ylmethyl)-1H-pyrrol-2(5H)-one **26.**

Yield: 54% (0.10 g); yellow solid; mp 190 °C. ^{1}H NMR ($CDCl_3$, 300 MHz): *δ* 8.28 (d, *J* = 3.6, 1H), 8.13 (s, 1H), 7.37-7.35 (m, 3H), 7.30-7.28 (m, 2H), 7.10-7.08 (m, 1H), 7.01-6.97 (m, 1H), 4.70 (br s, 2H), 4.68 (s, 1H), 4.44 (d, *J* = 14.7, 1H), 4.41 (br s, 1H), 4.38 (br s, 1H), 4.34 (d, *J* = 15.0, 1H), 4.19 (br s, 5H), 4.13 (br s, 1H), 4.10 (br s, 1H), 3.18 (d, *J* = 14.1, 1H), 3.11 (d, *J* = 13.8, 1H), 1.81 (s, 1H). ^{13}C NMR ($CDCl_3$, 75 MHz): *δ* 172.6, 169.8, 150.3, 147.7, 137.3, 134.2, 130.4, 128.8, 128.7, 128.0, 123.0, 94.3, 89.8, 84.6, 73.0, 70.5, 70.4, 68.65, 68.56, 68.1, 37.7, 37.3. HRMS (ESI^+): *m/z* calcd. for $[M + H]^+$ $C_{28}H_{27}FeN_2O_3$ 494.1287, found 494.1284.

4.1.2.8. 4-Benzyloxy-1-(ferrocenylethyl)-5-hydroxy-5-(4-trifluoromethylbenzyl)-1H-pyrrol-2(5H)-one **27.**

Yield: 21% (0.12 g); brownish solid; mp 112-114 °C. ^{1}H and ^{13}C NMR could not be recorded due to very low solubility. ^{19}F NMR ($CDCl_3$, 282 MHz): *δ* -62.9 (s). HRMS (ESI^+): *m/z* calcd. for $[M + H]^+$ $C_{31}H_{28}F_3FeNO_3$ 575.1365, found 575.1367.

4.1.2.9. 4-Benzyloxy-1-(ferrocenylpropyl)-5-hydroxy-5-(4-trifluoromethylbenzyl)-1H-pyrrol-2(5H)-one **28.**

Yield: 56% (0.16 g); yellow solid; mp 132-134 °C. ^{1}H NMR (CD_3OD, 300 MHz): *δ* 7.49-7.39 (m, 7H), 7.22-7.20 (m, 2H), 5.05-4.87 (m, 3H), 4.11-4.10 (m, 7H), 4.05-4.04 (m, 2H), 3.59-3.56 (m, 1H), 3.26-3.25 (m, 2H), 2.42-2.37 (m, 2H), 2.01-1.90 (m, 2H). ^{13}C NMR (CD_3OD, 75 MHz): not possible due to low solubility. ^{19}F NMR (CD_3OD, 282 MHz): -64.1 (s). HRMS (ESI^+): *m/z* calcd. for $[M + H]^+$ $C_{32}H_{29}F_3FeNO_3$ 589.1522, found 589.1490.

Typical procedure for the preparation of γ-lactams (**29**-**30**). Starting from lactone **19**, the same procedure of lactam **24** was used except that $Fc(CH_2)_nNH_2$ (1.2 equiv.) was replaced by 4-trifluoromethylbenzylamine (2 equiv.). Reaction mixture was vigorously stirred at 80°C in a sealed tube overnight. Solvent was then evaporated in vacuo and residue was purified by silica gel column chromatography (eluent: petroleum ether/AcOEt, 2:1) giving 0.25 g (yield: 90%) of lactam **30** as a brownish solid.

4.1.2.10. 4-Benzyloxy-5-hydroxy-1,5-bis(4-trifluoromethylbenzyl)-1H-pyrrol-2(5H)-one **29.**

Yield: 35% (64 mg); white solid; mp 137 °C. ^{1}H NMR ($CDCl_3$, 300 MHz): δ 7.51 (d, J = 8.1, 2H), 7.42 (d, J = 8.1, 2H), 7.38-7.32 (m, 4H), 7.28-7.26 (m, 3H), 6.93 (d, J = 8.1, 2H), 4.86 (s, 1H), 4.82 (s, 2H), 4.63 (d, J = 15.6, 1H), 4.49 (d, J = 15.6, 1H), 3.58 (s, 1H), 3.23 (d, J = 14.1, 1H), 3.12 (d, J = 14.1, 1H). ^{13}C NMR ($CDCl_3$, 75 MHz): δ 173.4, 170.6, 142.5, 138.0, 133.9, 129.9, 129.6 (q, J = 32.3), 129.5 (q, J = 32.3), 129.0, 128.8, 128.5, 127.9, 125.4 (q, J = 3.7), 124.9 (q, J = 3.8), 124.04 (q, J = 270.1), 123.98 (q, J = 270.4), 93.9, 90.1, 73.3, 41.6, 40.5. ^{19}F NMR ($CDCl_3$, 282 MHz): δ -62.5 (s), -62.6 (s). HRMS (ESI^+): *m/z* calcd. for $[M + Na]^+$ $C_{27}H_{21}F_6NNaO_3$ 544.1318, found 544.1318.

4.1.2.11. 4-Benzyloxy-5-(ferrocenemethyl)-5-hydroxy-1-(4-trifluoromethylbenzyl)-1H-pyrrol-2(5H)-one **30.**

Yield 90% (0.25 g), brownish solid, mp 59-60 °C. ^{1}H NMR and ^{13}C NMR: not possible due to low solubility. ^{19}F NMR (CD_3OD, 282 MHz): δ -62.9 (s). HRMS (ESI^+): *m/z* calcd. for $[M + H]^+$ $C_{30}H_{27}F_3FeNO_3$ 561.1209, found 561.1193.

*4.1.3. Synthesis of lactams **31**-**34***

Typical procedure for the preparation of γ-lactams (**31**-**34**). To a solution of lactam **24** (30 mg, 0.053 mmol) in anhydrous CH_2Cl_2 (3.0 mL) was added a solution *p*-toluenesulfonic acid (PTSA, 1.01 mg, 0.0053 mmol) in anhydrous methanol (3 mL). Reaction mixture was then heated at 50-60 °C in a sealed tube for 2h. Solvents were then evaporated in vacuo and residue was purified by silica gel column chromatography (eluent: petroleum ether/AcOEt, 2:1) giving 28 mg (yield: 92%) of lactam **31** as a yellow solid.

4.1.3.1. 4-Benzyloxy-5-methoxy-1-(ferrocenemethyl)-5-(4-trifluoromethylbenzyl)-1H-pyrrol-2(5H)-one **31.**

Yield: 92% (28 mg); yellow solid; mp 161 °C. ^{1}H NMR ($CDCl_3$, 300 MHz): δ 7.37-7.34 (m, 5H), 7.28-7.26 (m, 2H), 6.97 (d, *J* = 7.2, 2H), 4.89 (s, 1H), 4.82 (d, *J* = 11.4, 1H), 4.74 (d, *J* = 11.7, 1H), 4.44 (br s, 1H), 4.40 (br s, 1H), 4.30 (br s, 2H), 4.22 (br s, 5H), 4.19-4.17 (m, 2H), 3.25 (d, *J* = 13.2, 1H), 3.16 (d, *J* = 13.2, 1H), 2.84 (s, 3H). ^{13}C NMR ($CDCl_3$, 75 MHz): δ 169.8, 169.5, 138.3, 134.2, 130.1, 129.1 (q, *J* = 34.1), 128.9, 128.8, 124.8 (q, *J* = 3.8), 124.1 (q, *J* = 270.4), 96.9, 94.5, 84.0, 73.0, 70.7, 70.4, 68.6, 68.4, 68.2, 51.0, 40.0, 37.4. ^{19}F NMR ($CDCl_3$, 282 MHz): δ -62.5 (s). HRMS (ESI^+): *m/z* calcd. for $[M + Na]^+$ $C_{31}H_{28}F_3FeNNaO_3$ 598.1263, found 598.1254.

4.1.3.2. 4-Benzyloxy-1-(ferrocenemethyl)-5-propyloxy-5-(4-trifluoromethylbenzyl)-1H-pyrrol-2(5H)-one **32.**

Yield: 39% (21 mg); yellow solid; mp 110 °C. ^{1}H NMR ($CDCl_3$, 300 MHz): δ 7.38-7.26 (m, 7H), 6.96 (d, *J* = 8.1, 2H), 4.87 (s, 1H), 4.79 (d, *J* = 11.7, 1H), 4.70 (d, *J* = 11.7, 1H), 4.44 (br s, 1H), 4.36 (br s, 1H), 4.38 (d, *J* = 14.7, 1H), 4.28 (d, *J* = 15.0, 1H), 4.20 (br s, 5H), 4.15 (br s, 1H), 4.11 (br s, 1H), 3.23 (d, *J* = 13.8, 1H), 3.16 (d, *J* = 13.8, 1H), 2.88 (t, *J* = 6.9, 2H), 1.53-1.43 (m, 2H), 0.84 (t, *J* = 7.5, 3H). ^{13}C NMR ($CDCl_3$, 75 MHz): δ 170.0, 169.8, 138.4, 134.2, 130.2, 129.0 (q, *J* = 32.0), 128.8, 128.7, 128.0, 124.71 (q, *J* = 3.8), 124.66 (q, *J* = 260.9), 96.5, 93.9, 84.2, 72.8, 70.7, 70.2, 68.6, 68.3, 68.2, 64.9, 40.2, 37.4, 22.5, 10.5. ^{19}F NMR ($CDCl_3$, 282 MHz): δ -62.4 (s). HRMS (ESI^+): *m/z* calcd. for $[M + Na]^+$ $C_{33}H_{32}F_3FeNNaO_3$ 626.1576, found 626.1569.

4.1.3.3. 4-Benzyloxy-5-(2-methoxyethoxy)-1-(ferrocenemethyl)-5-(4-trifluoromethylbenzyl)-1H-pyrrol-2(5H)-one **33.**

Yield: 75% (50 mg); yellow solid; mp 135 °C. ^{1}H NMR ($CDCl_3$, 300 MHz): δ 7.38-7.28 (m, 7H), 6.95 (d, *J* = 7.8, 2H), 4.87 (s, 1H), 4.80 (d, *J* = 11.7, 1H), 4.71 (d, *J* = 11.7, 1H), 4.49 (br s, 1H), 4.43 (br s, 1H), 4.33 (br s, 2H), 4.24 (br s, 5H), 4.19 (br s, 1H), 4.15 (br s, 1H), 3.39-3.33 (m, 5H), 3.30 (d, *J* = 14.7, 1H), 3.22 (d, *J* = 14.1, 1H), 3.18-3.06 (m, 2H). ^{13}C NMR ($CDCl_3$, 75 MHz): δ 169.73, 169.66, 138.2, 134.1, 130.1, 129.0 (q, *J* = 33.9), 128.9, 128.7, 128.1, 124.8 (q, *J* = 3.5), 124.1 (q, *J* = 270.3), 96.7, 94.1, 73.0, 71.1, 69.4, 69.0, 62.5, 59.0, 39.9, 37.5. ^{19}F NMR ($CDCl_3$, 282 MHz): δ -62.5 (s). HRMS (ESI^+): *m/z* calcd. for $[M + Na]^+$ $C_{33}H_{32}F_3FeNNaO_4$ 642.1526, found 642.1516.

4.1.3.4. 4-Benzyloxy-5-(2-(tert-butoxycarbonylamino)ethoxy)-1-(ferrocenemethyl)-5-(4-trifluoromethylbenzyl)-1H-pyrrol-2(5H)-one **34.**

Yield: 62% (55 mg); yellow solid; mp 70 °C. ^{1}H NMR ($CDCl_3$, 300 MHz): δ 7.4 (m, 5H), 7.3 (m, 2H), 7.01 (m, 2H), 4.92 (s, 1H), 4.84 (d, *J* = 11.4, 1H), 4.73 (m, 1H), 4.5-4.1 (m, 11H), 3.3-2.8 (m, 7H), 1.47 (s, 9H). ^{13}C NMR ($CDCl_3$, 75 MHz): δ 170.6, 169.5, 155.7, 138.1, 134.0, 130.1, 129.2 (q, *J* = 30.6), 129.0, 128.8, 128.1, 124.9 (q, *J* = 3.7), 124.1 (q, *J* = 270.3), 96.8, 94.0, 84.0, 79.3, 73.1, 70.5, 70.2, 68.7, 68.5, 68.3, 62.6, 40.0, 39.8, 37.5, 28.4. ^{19}F NMR ($CDCl_3$, 282 MHz): δ -62.5 (s). HRMS (ESI^+): *m/z* calcd. for $[M + Na]^+$ $C_{37}H_{39}F_3FeN_2NaO_5$ 727.2058, found 727.2048.

*4.1.4. Synthesis of lactams **35-36***

Typical procedure for the preparation of γ-lactams (**35-36**). To a suspension of sodium hydride (5.70 mg, 0.142 mmol) in dry THF (1.5 mL) under argon atmosphere at 0°C, was added dropwise lactam **24** (40 mg, 0.071 mmol) in THF (1.0 mL). After stirring at 0 °C for 5 min., ethyl bromoacetate (39 μL, 0.355 mmol) was added. Reaction mixture was allowed to reach room temperature, then was stirred for 1h. After addition of water (5 mL), the reaction mixture was extracted with ethyl acetate (10 mL). Solvents were then evaporated in vacuo and residue

was purified by silica gel column chromatography (eluent: petroleum ether/AcOEt, 2:1) giving 40 mg (yield: 87%) of lactam **35** as a yellow solid.

4.1.4.1. Ethyl 2-(3-benzyloxy-1-(ferrocenemethyl)-5-oxo-2-(4-trifluoromethylbenzyl)-2,5-dihydro-1H-pyrrol-2-yloxy)acetate **35.**

Yield: 87% (40 mg); yellow solid; mp 90 °C. ^{1}H NMR ($CDCl_3$, 300 MHz): δ 7.40-7.36 (m, 5H), 7.25 (d, J = 7.8, 2H), 7.05 (d, J = 7.8, 2H), 4.90 (s, 1H), 4.81 (d, J = 11.7, 1H), 4.73 (d, J = 11.7, 1H), 4.55 (d, J = 14.7, 1H), 4.41 (s, 1H), 4.33 (s, 1H), 4.21-4.16 (m, 6H), 4.14-4.09 (m, 3H), 4.06 (s, 1H), 3.51 (d, J = 15.0, 1H), 3.41-3.30 (m, 3H), 1.23 (t, J = 7.2, 3H). ^{13}C NMR ($CDCl_3$, 75 MHz): δ 169.2, 169.0, 168.6, 138.0, 133.9, 130.1, 129.3 (q, J = 32.2), 129.0, 128.0, 125.0 (q, J = 3.8), 124.0 (q, J = 270.5), 96.9, 94.2, 83.7, 73.1, 70.22, 70.16, 68.6, 68.5, 68.1, 61.0, 60.9, 39.6, 37.6, 14.1. ^{19}F NMR ($CDCl_3$, 282 MHz): δ -62.5 (s). HRMS (ESI^+): *m/z* calcd. for $[M + Na]^+$ $C_{34}H_{32}F_3FeNNaO_5$ 670.1475, found 670.1459.

4.1.4.2. 2-(3-Benzyloxy-1-(ferrocenemethyl)-5-oxo-2-(4-trifluoromethylbenzyl)-2,5-dihydro-1H-pyrrol-2-yloxy)-acetonitrile **36.**

Yield: 32% (10.5 mg); yellow solid; mp 174-176 °C. ^{1}H NMR ($CDCl_3$, 300 MHz): δ 7.46-7.35 (m, 7H), 7.08 (d, J = 7.8, 2H), 4.99 (s, 1H), 4.95 (d, J = 11.1, 1H), 4.75 (br s, 1H), 4.71 (d, J = 11.1, 1H), 4.44 (br s, 1H), 4.23 (br s, 6H), 4.18 (br s, 2H), 3.99 (d, J = 14.4, 1H), 3.45 (s, 2H), 3.35 (d, J = 14.1, 1H), 3.27 (d, J = 13.8, 1H). ^{13}C NMR ($CDCl_3$, 75 MHz): δ 169.1, 168.2, 137.3, 133.6, 130.0, 129.6 (q, J = 32.8), 129.2, 128.82, 128.76, 125.2 (q, J = 3.6), 123.9 (q, J = 271.1), 115.9, 97.1, 94.7, 83.2, 73.4, 70.0, 69.8, 69.0, 68.7, 68.3, 48.4, 38.4, 37.6. ^{19}F NMR ($CDCl_3$, 282 MHz): δ -62.5 (s). HRMS (ESI^+): *m/z* calcd. for $[M + Na]^+$ $C_{32}H_{27}F_3FeN_2NaO_3$ 623.1216, found 623.1202.

*4.1.5. Synthesis of lactam **37***

Typical procedure for the preparation of γ-lactam (**37**). To a solution of lactam **24** (22.0 mg, 0.040 mmol) and *N*,*N*-(dimethylamino)pyridine (DMAP, 0.05 mol %) in anhydrous CH_2Cl_2 (1.0 mL), was added dropwise acetic anhydride (30 μL, 0.32 mmol). Reaction mixture was then stirred at room temperature for 30 min. Solvent was then evaporated in vacuo and residue was purified by silica gel column chromatography (eluent: petroleum ether/AcOEt, 2:1) giving 19 mg (yield: 80%) of lactam **37** as a yellow solid.

4.1.5.1. **3-Benzyloxy-1-(ferrocenemethyl)-5-oxo-2-(4-trifluoromethylbenzyl)-2,5-dihydro-1*H*-pyrrol-2-yl acetate (37).** Yield: 80% (19.3 mg); yellow solid; mp 135 °C. ^{1}H NMR ($CDCl_3$, 300 MHz): δ 7.42-7.38 (m, 5H), 7.26 (br s, 2H), 7.03 (d, J = 7.5, 2H), 4.90 (s, 1H), 4.86 (d, J = 11.4, 1H), 4.69 (d, J = 11.4, 1H), 4.61 (br s, 1H), 4.41-4.33 (m, 3H), 4.26 (br s, 5H), 4.18 (br s, 2H), 3.34 (d, J = 13.8, 1H), 3.18 (d, J = 13.5, 1H), 1.83 (s, 3H). ^{13}C NMR ($CDCl_3$, 75 MHz): δ 170.1, 169.6, 167.4, 136.9, 134.2, 130.2, 129.1 (q, J = 34.1), 128.9, 128.7, 128.2, 125.0 (q, J = 3.7), 122.0 (q, J = 268.4), 95.4, 91.9, 73.2, 69.3, 39.7, 37.8, 21.4. ^{19}F NMR ($CDCl_3$, 282 MHz): δ -62.5 (s). HRMS (ESI^+): *m/z* calcd. for $[M + Na]^+$ $C_{32}H_{28}F_3FeNNaO_4$ 626.1212, found 626.1240.

5. Materials and methods.

5.1. Cyclic voltammetry

Electrochemical measurements were performed using an EG & G-Princeton Applied Research 263A all-in-one potentiostat, using a standard three-electrode setup with a glassy carbon electrode (working electrode, diameter = 3 mm), platinum wire auxiliary electrode and a non-aqueous Ag/Ag^+ (0.01M $AgNO_3$ + 0.1M *n*-Bu_4NClO_4) system in acetonitrile as the reference electrode. All solutions under the study were 0.1 M in the supporting electrolyte *n*-Bu_4NPF_6 (Fluka *puriss* electrochemical grade) with the voltage scan rate of 0.2 V s^{-1}. Anhydrous CH_3CN was obtained from Fisher Scientific. Solutions (2.5 mL) were thoroughly bubbled with dry argon for 15 minutes to remove oxygen before any experiment and kept under positive pressure of argon. Under these experimental conditions the ferrocene/ferricinium couple, used as internal reference for potential measurements, was located at $E_{1/2}$ = + 0.09 V in CH_3CN. Origin 7.0 was used to process the analytical results.

5.2. Physico-Biochemical studies

Distilled water was purified by passing it through a mixed bed of ion-exchanger (Bioblock Scientific R3-83002, M3-83006) and activated carbon (Bioblock Scientific ORC-83005). DMSO (E. Merck, Uvasol, for spectroscopy or Sigma, Bioreagent, for molecular biology), acetonitrile (E. Merck Uvasol, for spectroscopy or HPLC quality 99.9% Chromasolv, Sigma Aldrich), chloroquine (Sigma, diphosphate salt), hydrogen peroxide (H_2O_2, 30% mass, Sigma Aldrich), hydrochloric acid (HCl 37% p.a., Prolabo), ferrocene (**Fc**, 98%, Sigma Aldrich), Fe(II) chloride (tetrahydrate, puriss, > 99%, Fluka) and methylene blue (trihydrate, molecular biology, Sigma Aldrich) were obtained from commercial suppliers and used without further purification. All stock solutions were prepared using an AG 245 Mettler Toledo analytical balance. Hematin (Fe^{III}PPIX(OH)) solution was prepared from hemin equine Type III (Fe^{III}PPIXCl, Sigma-Aldrich) and 0.1 M NaOH solution vigorously stirred at room temperature (RT) for 1 h. The $[Fe^{III}PPIX]_0$ was calculated from the molecular weight of the corresponding monomers. Hepes (2-[4-(2-hydroxyethyl)piperazin-1-yl]ethanesulfonic acid, Gerbu Biotechnik) buffer (0.2 M) was prepared in water and the pH (7.5) was adjusted with NaOH slurry. pH reading was done on a PHM240 MeterLab® millivoltmeter fitted with a combined glass electrode (Metrohm 6.0234.500, Long Life, 0.1 m NaCl). Calibration was done with commercial Merck® buffers (1.68, 4.00, 6.86, 7.41, and 9.18). Stock solutions of the substrates in DMSO for the different assays were freshly prepared in Eppendorf tubes just before the experiments.

Spectrophotometric titration of hematin π-π dimer by the substrates. The experimental conditions related to the spectrophotometric titration of haematin π-π dimer by the substrates are available in reference [21]. An aliquot of 10 µL of the Fe^{III}PPIX(OH) stock solution (~ 2 mM) was dissolved in 500 µL 0.2 M sodium hepes buffer at pH 7.5 in a 0.2 cm Hellma optical cell. The absorption spectrophotometric titrations were carried out by adding microvolumes of a stock solution of the substrate (~ 8×10^{-4} M in DMSO). Aliquots of 1-20 µL of the stock substrate solution were successively added to the reaction mixture and, after each addition, a UV-visible absorption spectrum (300 nm < λ < 800 nm) was recorded with an Agilent CARY 5000 spectrophotometer. Special care was taken to ensure that equilibrium was attained. The association constants K_A and the stoichiometries of the species at equilibrium were determined by processing the spectrophotometric data with the Specfit program [36-41]. Specfit uses factor analysis to reduce the absorbance matrix and to extract the eigenvalues prior to the multiwavelength fit of the reduced data set according to the Marquardt algorithm. The

uncertainties on the log *K* values are given as σ with σ = standard deviation. Origin 7.0 was used to process the analytical results.

Catalyzing properties in the Fenton reaction probed by methylene blue. The capacity of the substrates to act as efficient catalysts to trigger the Fenton reaction in the presence of H_2O_2 was monitored by absorption spectrophotometry with the help of a chromogenic reporter, the methylene blue (**MB**) dye, which is well known to undergo oxidative bleaching upon reaction with Fe^{II}(Fc)/H_2O_2 (Fc = ferrocene) catalytic system. Solutions at pH 3 were prepared by dilution of hydrochloric acid (HCl 37% p.a., Prolabo) and the pH was ascertained by pH-metry. An acidic milieu (pH 3) was chosen because the oxidative degradation of MB by hydroxyl radicals •OH generated through the Fenton reaction was found to be optimal and almost quantitative under these experimental conditions [28]. The stock solution of **MB** (5 mM) was freshly prepared in water, while those of the ferrocene-based molecules (2.5 mM) were prepared in CH_3CN and kept at 4°C. The stock solution of H_2O_2 (3.26 ± 0.03 M) was assayed by colorimetric titration with $KMnO_4$ (Fluka) under acidic conditions (H_2SO_4). Ferrous chloride solutions were titrated spectrophotometrically at 510 nm by using 1,10-phenanthroline in a reducing milieu (hydroxylamine). Typically, the stock solution of **MB** (3 µL, final concentration of 3×10^{-5} M) were introduced in 473 µL of the acidic aqueous solution at pH 3 in an optical quartz suprasil cell of 2 mm of optical pathlength. An aliquot of 19 µL of the ferrocene-based substrate (9.5×10^{-5} M) was quickly added. The Fenton reaction (i.e. generation of the scavenging hydroxyl •OH radical) was triggered by addition of 5 µL (final concentration of 3.26 x 10^{-2} M; $[H_2O_2]_0$/[Fe catalyst]$_0$ ~ 340) of concentrated H_2O_2 solution. The fading kinetics of **MB** upon oxidation/degradation with •OH was monitored by recording UV-visible absorption spectra as a function of time (scanning kinetics mode with each spectrum of spectral range of 400-800 nm recorded each 3 minutes over a 4 hours period) with an absorption spectrophotometer (Varian Cary 50). The 2 mm optical quartz cell was maintained at 37°C all over the experiment (temperature regulated and controlled with a Vary Cary Single Cell Peltier Accessory). The kinetic data were processed with the Specfit program [36-41]. Origin 7.0 was used to process the analytical results [42].

5.3. Single-crystal X-ray diffraction

Single-crystal X-ray studies of **24, 31** and **33** were carried out by using a Gemini diffractometer and the related analysis software [43]. An absorption correction based on the crystal faces was applied to the data sets (analytical) [44, 45]. The structure was solved by direct methods using the SIR97 program [46] combined with Fourier difference syntheses and refined against F using

reflections with [I/σ(I) > 3] by using the CRYSTALS program [47]. All atomic displacement parameters for non-hydrogen atoms were refined with anisotropic terms. The hydrogen atoms were theoretically located on the basis of the conformation of the supporting atom and refined by using the riding model. X-ray diffraction crystallographic data and refinement details for complexes **24**, **31** and **33** are summarized in Table S2, ESI. CCDC-2042047 (**24**), -2042046 (**31**) and -2042045 (**33**) contain the supplementary crystallographic data for this paper. These data can be obtained free of charge from The Cambridge Crystallographic Data Centre.

5.4. In vitro anti-plasmodial assay

The in vitro drug sensitivity assay with cultured parasites, IC_{50} determination by the SYBR Green I assay and cytotoxicity were determined as reported in reference [19].

5.5. In vivo anti-plasmodial assay

Ethical clearance

All experiments were conducted in accordance with the guidelines of the European Council Directive (2010/63/UE) and with French laws and regulations (Articles R214-87 to R214-137 of the Rural Code and decree n°2013-118 dated February 1, 2013 published on February 7, 2013). All experimental procedures, were evaluated and approved by the Ministry of Higher Education and Research (APAFIS# 01069-02 Notification). Mice procedures were evaluated by the ethical clerance committee of the Val de Loire (CEEA VdL, committee number n°19) and took place at INRAE Experimental Infection Platform PFIE (https://www6.val-de-loire.inrae.fr/pfie_eng/).

After a seven days acclimation period, 80 CBA/J mice (5 mice / group) were administered 200 µL of the tested compound by gavage. Three doses were tested from 5 to 50 mg/kg once. Control groups received physiological serum (negative control) or DMSO (solvent control). For repeated toxicity experiments, this treatment was repeated 3 times on 3 successive days.

Blood samples (200µL) were collected at D0, D1, D2 and D3. Safety was tested with a panel of biomarkers (albumin, cholesterol, globin, glucose, alkaline phosphatase, total proteins and urea) using Select-6V rings with the M-ScanII Biochemical analyzer (Melet Schloesing Laboratories, France).

After acclimation, 6 weeks old CBA/J mice of were challenged with intraperitoneal administration of 10^6 *Plasmodium berghei* ANKA infected red blood cells as described [48]. Mice were treated at day five post-infection. Mice were administered 400 µL of the tested compound by gavage once a day for 3 days. Control groups received either: 1) *Plasmodium* parasites IP + oral artesunate ; 2) *Plasmodium* parasites IP + oral PBS ; 3) PBS IP + oral PBS ; 4) *Plasmodium* parasites IP + oral Oil/ethanol. Test groups received: 5) *Plasmodium* parasites

IP + oral 5 mg/kg tested compound; 6) *Plasmodium* parasites IP + oral 50 mg/kg tested compound.

The clinical follow-up (weight and clinical staging) was carried out daily: same biomarkers used for the safety experiments were tested for the challenge experiments.

From day 5 to day 12, blood was collected in the tail vein to measure the parasitemia The experiment end-point was day 12 post-infection.

6. Acknowledgements

This work was supported in part by Agence Nationale de la Recherche (grant ANR-11-EMMA-04-QUINOLAC), the Centre National de la Recherche Scientifique (CNRS), the Université Lyon 1, the Université de Strasbourg, the Laboratoire d'Excellence (LabEx) ParaFrap (grant LabEx ANR-11-LABX-0024 to E.D.-C), the l'Institut National de Recherche pour l'Agriculture, l'Alimentation et l'Environnement (INRAE) and the Ministère de l'Enseignement Supérieur et de la Recherche (Ph.D fellowship to S. I.). The authors thank also the Consortium Antiparasitaire et Fongique (CaPF) for support, the Centre Commun de Spectrométrie de Masse (CCSM) and Centre Commun de RMN (CCRMN) of Université Lyon 1 for their assistance and access to the facilities.

7. References

[1] P. Shetty, The numbers game, Nature 484 (2012) S14-S15.

[2] M. Schlitzer, Antimalarial drugs - what is in use and what is in the pipeline, Arch. Pharm. Chem. Life. Sci. 341 (2008) 149-163.

[3] M. A. Biamonte, J. Wanner, R. G. Le Roch, Recent advances in malaria drug discovery, Bioorg. Med. Chem. Lett. 23 (2013) 2829-2843.

[4] C. Teixeira, N. Vale, B. Pérez, A. Gomes, J. R. B. Gomes, P. Gomes, "Recycling" classical drugs for malaria, Chem. Rev. 114 (2014) 11164-111220.

[5] L.-S. Feng, Z. Xu, L. Chang, L. Chuan, Y. X.-Fei, C. Gao, D. Chuan, C. Ding, F. Zhao, F. Shi, W. Feng, X. Wu, Hybrid molecules with potential in vitro antiplasmodial and in vivo antimalarial activity against drug-resistant Plasmodium falciparum, Med. Res. Rev. 40 (2020), 931-997.

[6] T. N. C. Wells, R. H. Van Huijsduijnen, W. C. Van Voorhis, Malaria medicines: a glass half full? Nature Rev. Drug Discov. 14 (2015) 424-442.

[7] A. C. Aguiar, L. R. F. de Sousa, C. R. S. Garcia, G. Oliva, R.V.C. Guido, New Molecular Targets and Strategies for Antimalarial Discovery, Curr. Med. Chem. 26 (2019) 4380-4402.

[8] N. Chopin, S. Iikawa, J. Bosson, A. Lavoignat, G. Bonnot, A.-L. Bienvenu, S. Picot, J.-P. Bouillon, M. Médebielle, 7-Chloro-4-aminoquinoline γ-hydroxy-γ-lactams derived-tetramates as a new family of antimalarial compounds, Bioorg. Med. Chem. Lett. 26 (2016) 5308-5311.
[9] S. Picot, P. M. Loiseau, A.-L. Bienvenu, New Anti-Malarial Drugs: Who Cares? Curr. Top. Med. Chem, 14 (2014) 1637-1642.
[10] D. Murugesan, M. Kaiser, K.L. White, S. Norval, J. Riley, P. G. Wyatt, S. A. Charman, K. D. Read, C. Yeates, I. H. Gilbert, Structure-activity relationship studies of pyrrolone antimalarial agents, ChemMedChem 8 (2013) 1537-1544.
[11] L. M. Coronado, C. T. Nadovich, C. Spadafora, Malarial hemozoin: from target to tool. Biochim Biophys Acta. 1840 (2014) 2032-2041.
[12] N. Chopin, H. Yanai, S. Iikawa, G. Pilet, J.-P. Bouillon, M. Médebielle, A rapid entry to diverse γ-ylidenetetronate derivatives through regioselective bromination of tetronic acid derived γ-lactones and metal-catalyzed postfunctionalization, Eur. J. Org. Chem. (2015) 6259-6269.
[13] C. Biot, G. Glorian, L. A. Maciejewski, J. S. Brocard, Synthesis and antimalarial activity in vitro and in vivo of a new ferrocene-chloroquine analogue, J. Med. Chem. 40 (1997) 3715-3718.
[14] Y. Adoke, R. Zoleko-Manego , S. Ouoba , A. B. Tiono, G. Kaguthi, J. E. Bonzela, T. T. Duong, A. Nahum, M. Bouyou-Akotet, B. Ogutu, A. Ouedraogo, F. Macintyre, A. Jessel, B. Laurijssens, M. H. Cherkaoui-Rbati, C. Cantalloube, A. C. Marrast, R. Bejuit , D. White, T. N. C. Wells, F; Wartha, D. Leroy, A. Kibuuka, G. Mombo-Ngoma, D. Ouattara, I. Mugenya, B. Q. Phuc, F. Bohissou, D. P. Mawili-Mboumba, F. Olewe, I. Soulama , H. Tinto H, on behalf of the FALCI Study Group, A randomized, double-blind, phase 2b study to investigate the efficacy, safety, tolerability and pharmacokinetics of a single-dose regimen of ferroquine with artefenomel in adults and children with uncomplicated Plasmodium falciparum malaria, Malar J. 19 (2021) 222.
[15] J. Xiao, Z. Sun, F. Kong, F. Gao, Current scenario of ferrocene-containing hybrids for antimalarial activity, Eur. J. Med. Chem. 185 (2020) 111791-111802.
[16] M. Mbaba, L. M. K Dingle, A. I. Zulu, D. Laming , T. Swart , J. A. de la Mare, H. C. Hoppe, A. L. Edkins, S. D. Khanye, Coumarin-Annulated Ferrocenyl 1,3-Oxazine Derivatives Possessing In Vitro Antimalarial and Antitrypanosomal Potency, Molecules. 26 (2021) 1333.
[17] X. Nqoro, B. A. Aderibigbe, 4-Aminoquinoline-ferrocene Hybrids as Potential Antimalarials. Recent Pat Antiinfect Drug Discov. 15 (2020) 157-172.

[18] M. Tonelli , E. Gabriele , F. Piazza, N. Basilico , S. Parapini , B. Tasso, R. Loddo, F. Sparatore, A. Sparatore, Benzimidazole derivatives endowed with potent antileishmanial activity. J. Enzyme Inhib. Med. Chem. 33 (2018) 210-226.
[19] D. Cornut, H. Lemoine, O. Kanishchev, E. Okada, F. Albrieux, A. H. Beavogui, A.-L. Bienvenu, S. Picot, J.-P. Bouillon, M. Médebielle, Incorporation of a 3-(2,2,2-trifluoroethyl)-γ-hydroxy-γ-lactam motif in the side chain of 4-aminoquinolines. Syntheses and antimalarial activities, J. Med. Chem. 56 (2013) 73-83.
[20] N. Chavain, H. Vezin, D. Dive, N. Touati, J.-F. Paul, E. Buisine, C. Biot, Investigation of the redox behavior of ferroquine, a new antimalarial, Mol. Pharmaceutics 5 (2008) 710-716.
[21] L. Johann, D. A. Lanfranchi, E. Davioud-Charvet, M. Elhabiri, A physico-biochemical study on potential redox-cyclers as antimalarial and anti-schistosomal drug, Curr. Pharm. Des. 18 (2012) 3539-3566.
[22] W. Friebolin, B. Jannack, N. Wenzel, J. Furrer, T. Oeser, C. P. Sanchez, M. Lanzer, V. Yardley, K. Becker, E. Davioud-Charvet, Antimalarial dual drugs based on potent inhibitors of glutathione reductase from Plasmodium falciparum, J. Med. Chem. 51 (2008) 1260-1277.
[23] O. Blank, E. Davioud-Charvet, M. Elhabiri, Interactions of the antimalarial drug methylene blue with methemoglobin and heme targets in Plasmodium falciparum: a physico-biochemical study, Antioxid. Red. Signal. 17 (2012) 544-554
[24] N. Chavain, E. Davioud-Charvet, X. Trivelli, L. Mbeki, M. Rottmann, R. Brun, C. Biot, Antimalarial activities of ferroquine conjugates with either glutathione reductase inhibitors or glutathione depletors via a hydrolyzable amide linker. Bioorg. Med. Chem. 17 (2009) 8048-8059.
[25] M. Bielitza, D. Belorgey, K. Ehrhardt, L. Johann, D. A. Lanfranchi, V. Gallo, E. Schwarzer, F. Mohring, E. Jortzik, D. L. Williams, K. Becker, P. Arese, M. Elhabiri, E. Davioud-Charvet, Antimalarial NADPH-Consuming Redox-Cyclers As Superior Glucose-6-Phosphate Dehydrogenase Deficiency Copycats, Antioxid. Red. Signal. 22 (2015) 1337-1351.
[26] K. Bachhawat, C. J. Thomas, N. Surolia, A. Surolia, Interaction of chloroquine and its analogues with heme: An isothermal titration calorimetric study, Biochem. Biophys. Res. Commun. 276 (2000) 1075-1079.
[27] Q. Wang, S. Tian, J. Cun, P. Ning, Degradation of methylene blue using a heterogeneous Fenton process catalyzed by ferrocene, Desalin Water Treat. 28-30 (2013) 5821-5830.
[28] H. Bataineh, O. Pestovsky, A. Bakac. pH-induced mechanistic changeover from hydroxyl radicals to iron(IV) in the Fenton reaction. Chem. Sci. 3 (2012) 1594-1599.

[29] C. Biot, D. Taramelli, I. Forfar-Bares, L. A. Maciejewski, M. Boyce, G. Nowogrocki, J. S. Brocard, N. Basilico, P. Olliaro, T. J. Egan, Insights into the mechanism of action of ferroquine. Relationship between physicochemical properties and antiplasmodial activity. Mol Pharm. 2 (2005) 185-193.

[30] F. Dubar, S. Bohic, C. Slomianny, J.-C. Morin, P. Thomas, H. Kalamou, Y. Guérardel, P. Cloetens, J. Khalife, C. Biot, Chem. Commun. 48 (2012) 910-912.

[31] F. Dubar, S. Bohic, D. Dive, Y. Guerardel, P. Cloetens, J. Khalife, C. Biot, ACS Med. Chem. Lett. 3 (2012) 480-483.

[32] K. K. Ncokazi, T. J. Egan, A colorimetric high-throughput beta-hematin inhibition screening assay for use in the search for antimalarial compounds. Anal. Biochem. 338 (2005) 306-319.

[33] P. D. Beer, D. K. Smith, Tunable bis(ferrocenyl) receptors for the solution-phase electrochemical sensing of transition-metal cations, J . Chem. Soc., Dalton Trans., (1998) 417–423.

[34] C-H. Chen, T. A. Postlethwaite, J. E. Hutchison, E. T. Samulski, R. W. Murray, Electrochemical measurements of anisotropic diffusion in thin lyotropic liquid crystal films using interdigitated array electrodes, J. Phys. Chem. 99 (1995) 8804-8811.

[35] I. U. Khand, T. Lanez, P. L. Pauson, Ferrocene derivatives. Part 24. Synthesis of dihydro-2-pyridines and dihydro-3*H*-2-cyclopent[*c*]azepines by photolysis of their cyclopentadienyliron derivatives, J. Chem. Soc. Perkin Trans. I 1989, 2075-2078.

[36] H. Gampp, M. Maeder, C. J. Meyer, A. D. Zuberbühler, Calculation of equilibrium constants from multiwavelength spectroscopic data—I: Mathematical considerations, Talanta 32 (1985) 95-101.

[37] F. J. C. Rossoti, H. S. Rossoti, R. J.Whewell, The use of electronic computing techniques in the calculation of stability constants, J. Inorg. Nucl. Chem. 33 (1971) 2051-2065.

[38] H. Gampp, M. Maeder, C. J. Meyer, A. D. Zuberbühler, Calculation of equilibrium constants from multiwavelength spectroscopic data—II[1]32, 95.: Specfit: two user-friendly programs in basic and standard fortran 7, Talanta 32 (1985) 257-264.

[39] H. Gampp, M. Maeder, C. J. Meyer, A. D. Zuberbühler, Calculation of equilibrium constants from multiwavelength spectroscopic data—IV: Model-free least-squares refinement by use of evolving factor analysis, Talanta 33 (1986) 943-951.

[40] D. W. Marquardt, An Algorithm for Least-Squares Estimation of Nonlinear Parameters, J. Soc. Indust. Appl. Math. 11 (1963) 431-441.

[41] M. Maeder, A. D. Zuberbühler, Nonlinear least-squares fitting of multivariate absorption data, Anal. Chem. 62 (1990) 2220-2224.
[42] Microcal™ 7.0 SR1 Origin™, 2002; OriginLab Corporation: Northampton, MA, USA.
[43] CrysAlisPro, v. 1.171.33.46 (rel. 27-08-2009 CrysAlis171.NET), Oxford Diffraction Ltd., 2009.
[44] J. De Meulenaer, H. Tompa, The absorption correction in crystal structure analysis, Acta Crystallogr. 19 (1965)1014–1018.
[45] R. H. Blessing, An empirical correction for absorption anisotropy Acta Crystallogr., Sect. A: Found. Crystallogr. 51 (1995) 33-38.
[46] A. Altomare, M. C. Burla, M. Camalli, G. L. Cascarano, C. Giacovazzo, A. Guagliardi, A. G. G. Moliterni, G. Polidori, R. Spagna, SIR97: a new tool for crystal structure determination and refinement, J. Appl. Crystallogr. 32 (1999) 115–119.
[47] D. J. Watkin, C. K. Prout, J. R. Carruthers, P. W. Betteridge in CRISTAL Issue 11, Chemical Crystallography Laboratory, Oxford, 1999.
[48] A.-L. Bienvenu, S. Picot, Cerebral malaria: protection by erythropoietin, Methods Mol. Biol. 982 (2013) 315-324.